



---

# IS DARK MATTER MADE OF AXIONS?

---

March 9, 2017

## Abstract

This review investigates the axion and axion-like particles (ALPs) as candidates for dark matter. The types of ALPs and their properties are examined, followed by a review of ALPs as dark matter particle candidates. The current constraints are investigated alongside the possible detection methods in use today. Future experiments and expected improvements to sensitivity are also discussed, to summarise the prospects for the next generation of axion search experiments.

Hannah M. Wakeling

Supervised by Professor J. Monroe

# Contents

<b>1</b>	<b>Introduction</b>	<b>4</b>
<b>2</b>	<b>Theoretical background of axions and ALPs</b>	<b>4</b>
2.1	The strong CP problem . . . . .	5
2.2	Solutions to the strong CP problem . . . . .	6
2.3	Axion models . . . . .	6
2.3.1	Dine-Fischler-Srednicki-Zhitnitskii (DFSZ) Axion Models . . . . .	7
2.3.2	Kim-Shifman-Vainstein-Zakharov (KSVZ) Axion Models . . . . .	8
2.4	Axion mass and coupling . . . . .	8
2.4.1	Axion mass . . . . .	8
2.4.2	Axion-photon coupling . . . . .	9
2.4.3	Axion-electron coupling . . . . .	9
2.4.4	Axion-nucleon coupling . . . . .	10
2.5	ALPs . . . . .	10
<b>3</b>	<b>Axions as candidates for dark matter</b>	<b>10</b>
3.1	Cold Dark Matter Axion Production Mechanisms . . . . .	13
3.2	Axions as a Bose-Einstein Condensate . . . . .	14
<b>4</b>	<b>Astrophysical sources of axions and ALPs</b>	<b>15</b>
4.1	Primakoff production . . . . .	16
4.2	Compton-like scattering . . . . .	18
4.3	Bremsstrahlung . . . . .	18
4.4	Axio-recombination and axio-deexcitation . . . . .	19
4.5	Nuclear magnetic transition of $^{57}\text{Fe}$ nuclei . . . . .	20
<b>5</b>	<b>Constraints from astrophysics</b>	<b>20</b>
5.1	Stellar energy loss limits . . . . .	20
5.2	X-ray satellite . . . . .	21
5.3	Conversion of astrophysical photon fluxes . . . . .	21
<b>6</b>	<b>Laboratory searches for axions and ALPs</b>	<b>22</b>
6.1	Photon regeneration . . . . .	22
6.2	Birefringence and Dichroism . . . . .	24
6.3	Helioscopes . . . . .	26
6.4	Haloscopes . . . . .	29

6.4.1	The Microwave Cavity Haloscope . . . . .	29
6.4.2	Bragg diffraction scattering . . . . .	32
6.4.3	Searches in dark matter direct detection experiments . . . . .	33
<b>7</b>	<b>Prospects for axion and ALP searches in the near future</b>	<b>33</b>
7.1	Photon regeneration experiment improvements . . . . .	35
7.2	Helioscope improvements . . . . .	35
7.3	Haloscope improvements . . . . .	36
7.4	Detection using atomic transitions . . . . .	39
7.5	Detection using nuclear magnetic resonance (NMR) . . . . .	39
7.6	Direct detection experiments . . . . .	40
<b>8</b>	<b>Conclusions</b>	<b>41</b>

# 1 Introduction

The Standard Model (SM) of particle physics does not contain particles that are dark matter candidates. However, beyond the SM there are theories that predict very weakly coupled particles that are natural dark matter candidates. This review explores the theory, the production mechanisms, and the detection methods of the ultralight dark matter candidate called the ‘axion’. This pseudoscalar particle was postulated 40 years ago as a potential solution to the strong charge-parity (CP) problem in the SM. Section 2 investigates the theoretical basis for the axion, including the strong CP problem, axion properties, the two leading axions models, and ALPs.

Even though the axion was presented as a solution to the strong CP problem, the axion itself is an ideal cold dark matter candidate. This prospect motivates the majority of ALP search experiments today. Dark matter is not necessarily composed of one type of particle, as dynamical models predict a large number of dark matter species. This review focuses on axions and ALPs as candidates as they are considered to have strong motivations which are considered in Section 3 [1]. Depending on the order of the formation of the universe, there are different theorised production mechanisms of axions and ALPs. Section 3 reviews these and the resulting constraints imposed on dark matter. There are also astrophysical sources of axions and ALPs that have different production mechanisms than that of cold dark matter. These production mechanisms are reviewed in Section 4. Observation of astrophysical objects and events can be used to constrain axion and ALP parameters, and therefore reduce the window in which to search for them. This is considered in Section 5.

Axions are currently undetected as they are very weakly interacting particles. Methods of detection have to bypass this barrier, generally by having a very high sensitivity. A plethora of laboratory methods are employed in numerous terrestrial experiments to search for axions and ALPs. These are examined in Section 6. These experimental searches have constrained the theoretical parameters of axion and ALP models, however there are proposed experimental upgrades, along with new detection techniques, that plan to explore new parameter space. Section 7 reviews these improvements and new methods.

## 2 Theoretical background of axions and ALPs

The main theoretical motivation for the axion is the strong CP problem of Quantum Chromodynamics (QCD). QCD – the quantum field theory of strong interactions – exhibits an inconsistency between theory and observation in relation to charge-parity violation; this was christened “the strong CP problem” [2]. Section 2.1 presents this inconsistency and Section 2.2 investigates the axion as the solution to it. Section 2.3 briefly summarises the Dine-Fischler-Srednicki-Zhitnitskii

(DFSZ) and Kim-Shifman-Vainstein-Zakharov (KSVZ) axion models, which are the current leading axion models. Coupling possibilities are evaluated in Section 2.4, with the differences between axions and ALPs being examined in 2.5. An important parameter of the axion is the scale  $f_A$ , which enters both into the axion mass and its coupling to particles we can observe; this parameter is described in Section 2.4.1.

## 2.1 The strong CP problem

There are three types of symmetries in particle physics, where a system remains the same after transformation. These are: charge conjugation symmetry C, where a particle is replaced by its antiparticle; parity inversion symmetry P, where spacial coordinates are flipped; and time reversal symmetry T, where the direction of time is reversed. These are part of the CPT theorem, which declares that any Lorentz invariant local quantum field theory with a Hermitian Hamiltonian must have simultaneous C, P and T symmetry [3].

Within the theory of the SM, violation of CP symmetry (combined C and P symmetry) is allowed due to the existence, and mixing, of (at least) three families of quarks with different masses. In the SM, the generation of mass occurs via the Higgs mechanism [4]. If quarks were massless, there would be no family mixing and, therefore, no CP violation.

The strong CP problem is that strong interactions could have CP symmetry violations, however, non-conserving interactions have not been observed experimentally [5]. Strong interactions are, therefore, CP invariant (the symmetry is conserved), however, there seems to be no fundamental explanation as to why this should be.

CP violation is parametrised within the SM with an angle  $\theta$  in the QCD Lagrangian. The QCD Lagrangian is, in theory, a complete description of the strong interaction, however, it leads to equations that are particularly hard to solve [6]. The  $\theta$  term of the QCD Lagrangian is of the form:

$$\mathcal{L}_\theta = \theta \frac{\alpha_s}{8\pi} G_{A\mu\nu} \tilde{G}_A^{\mu\nu}, \quad (1)$$

where  $\alpha_s \sim 1$  is the coupling constant for the gluon field analogous to the fine structure constant  $\alpha$  [7],  $G_{A\mu\nu}$  is the gluon field strength, and  $\tilde{G}_A^{\mu\nu} = \frac{1}{2}\epsilon^{\mu\nu\alpha\beta}G_{A\alpha\beta}$  is its dual (with  $\epsilon^{0123} = 1$  being the totally antisymmetric tensor). The term  $\theta$  is the “sum of the independent contributions of the phase from QCD vacuum and a phase coming from the quark Yukawa couplings” [1]. In quantum field theory, a vacuum is the quantum state of the lowest possible energy of a field, and the vacuum state of QCD is a dense state of matter made of complexly interacting gauge fields and quarks [8]. Quark Yukawa couplings are the interaction between a scalar field and a Dirac field, and can be used to describe the coupling between the Higgs field, and massless quark and lepton fields in the SM [9].

The gluon density  $G_{A\mu\nu}\tilde{G}_A^{\mu\nu}$  violates P symmetry, but conserves C symmetry, which can produce a neutron electric dipole moment of order  $d_n \simeq \frac{em_q}{m_N^2}\theta$ , where  $e$  is the electron charge,  $m_q$  is the mass of the quark, and  $m_N$  is a typical hadronic scale that was chosen to be the nucleon mass.

The  $\theta$  term is expected to be of order one, however, the strong bound on the neutron electron dipole moment,  $d_n < 1.1 \times 10^{-26}$  ecm requires  $\theta < 10^{-10}$  [10]. This is the strong CP problem [1]; the value for  $\theta$  is extremely small and there is no natural explanation for it. It is considered to be a fine-tuning problem.

## 2.2 Solutions to the strong CP problem

One solution to the strong CP problem would be to assume that one of the quark masses is lighter than that of a neutrino. This, however, contradicts experiment, as seen in References [11, 12].

Another solution presents an argument that enables avoidance of the strong CP problem altogether. Banerjee *et al.* (2003) make the claim that it is natural to avoid CP violation by setting  $\theta$  equal to zero through the regularisation of QCD [5].

However, the solution that has been argued to be the only viable resolution [1], and the solution that this review focuses on, makes the  $\theta$  term irrelevant. Peccei and Quinn [11, 12] introduced this solution through a spontaneously broken global chiral symmetry called ‘ $U(1)_{PQ}$ ’ symmetry. This spontaneous breaking of  $U(1)_{PQ}$  symmetry gives rise to a psuedo-Nambu-Goldstone boson (NGB) [13], a boson discovered by Yoichiro Nambu in Bardeen–Cooper–Schrieffer (BCS) Superconductivity [14] and expanded on by Jeffrey Goldstone in “Field Theories with Superconductor Solutions” [15]. This particular NGB was named the ‘PQ axion’ or ‘QCD axion’. The additional symmetry allows the characteristic phase sum  $\theta$  to be replaced by a CP *conserving* interaction. This is the interaction of the axion field with the gluon density  $a(x)$  in the form:

$$\theta \rightarrow \frac{a(x)}{f_A}, \quad (2)$$

where  $f_A$  is the energy scale parameter, or ‘decay constant’, associated with the  $U(1)_{PQ}$  symmetry spontaneously breaking.

## 2.3 Axion models

The original axion model, the Peccei-Quinn-Weinberg-Wilczek (PQWW) model or ‘visible’ axion model [11, 13, 16], introduced one complex scalar field. It has now been experimentally excluded [2]. It used the low energy scale  $f_{weak}$ , which produces axions that are heavier than experimental constraints allow ( $m_A \sim 1 \times 10^5$  eV) [17]. However this did not rule out axions altogether.

Axions that arise from a higher symmetry-breaking energy scale  $f_A \gg f_{weak}$  are still possible. These axions have to: be very light, have a lifetime longer than that of the universe, and be very weakly coupled to normal matter and radiation. They have been named ‘invisible axions’ due to their weak coupling and as they have not yet been observed by laboratory experiments. Invisible axions have significant astrophysical and cosmological consequences, such as having the ability to form stable coherently oscillating axion fields, and playing an important role in the distribution of dark matter in the universe [18, 19, 20].

The DFSZ axion and the KSVZ axion are the two leading models of the invisible axion [21], and allow very specific ranges of coupling and mass parameter space. Figure 1 shows the variation of the axion-neutron, axion-electron, and axion-photon couplings for each model.

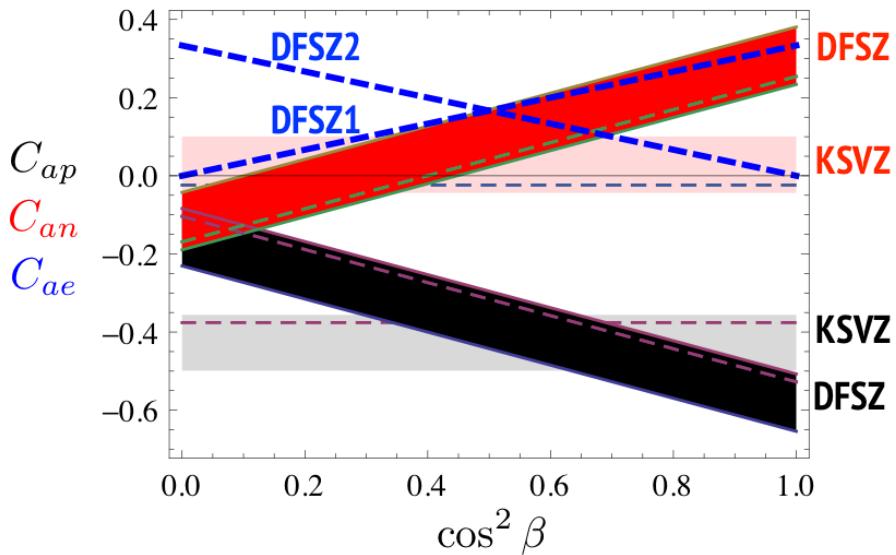


Figure 1: A graph of the axion-proton, axion-neutron and axion-electron couplings ( $C_{ap}$  black), ( $C_{an}$  red), and ( $C_{ae}$  blue) respectively) vs.  $\cos^2 \beta$  (a model dependent parameter), with low-energy-QCD error bars ( $m_u/m_d = 0.56^{+0.04}_{-0.26}$ ) in the KSVZ and DFSZ models [22]. Here  $C_{af}$  is the coupling normalised as  $C_{af} = g_{af} \times f_A/m_f$  where  $m_f$  is the mass of the fermion ( $\tan \beta$  is the ratio of extra Higgs fields in the model).

### 2.3.1 Dine-Fischler-Srednicki-Zhitnitskii (DFSZ) Axion Models

The DFSZ axion is a Grand Unified Theory (GUT) – a theory in which the three gauge interactions of the SM merge into a single force at a grand unification energy. In addition to the field introduced in the PQWW model, the DFSZ model adds an  $SU(2) \times U(1)$  singlet, which is a scalar field carrying Peccei-Quinn (PQ) charge. This allows SM quarks and leptons to couple to axions as they are also required to carry a PQ charge [21]. Therefore, the DFSZ axion

properties are beneficial to research as it's coupling is related to the properties of the known particles that couple to it [1].

### 2.3.2 Kim-Shifman-Vainstein-Zakharov (KSVZ) Axion Models

The KSVZ axion is a hadronic model. These axions only couple to heavy quarks and, like the DFSZ axion, the  $SU(2) \times U(1)$  singlet field carries a PQ charge. The main difference between these axions and DFSZ axions is that they do not couple to leptons or ordinary quarks at the tree-level, giving a strong suppression of the axion-electron coupling  $g_{Ae}$  [21]. Due to the axion-photon interaction (see Section 2.4.2) KSVZ axions can be coupled to electrons, however this is a higher order process and is extremely weak [23].

## 2.4 Axion mass and coupling

Axions can couple to a variety of matter particles, including: photons, electrons, nucleons, and gluons [24]. Recall from Section 2.3 that there is a model dependence of the axion couplings [21]. Figure 2 displays the Feynman diagrams along with the couplings to axions.

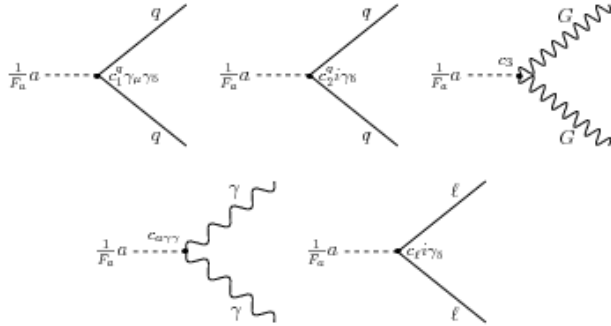


Figure 2: The Feynman diagrams of axion couplings to quarks  $q$ , gluons  $G$ , photons  $\gamma$  and leptons  $\ell$ , with couplings ( $c_3$  and  $c_{A\gamma\gamma}$  being anomalous couplings) [17]. Note the notation difference of the scale parameter  $F_a = f_A$ .

### 2.4.1 Axion mass

The coupling of axions to SM particles is suppressed by the scale factor  $f_A$ , mentioned in Section 2.1 [25]. In fact, all of the properties of the axion depend on this scale parameter. The value of  $f_A$  was originally bounded by astrophysical and cosmological observations to any value between the electroweak scale  $f_{weak} \sim 246$  GeV and the Planck mass of  $f_A \sim 10^{19}$  GeV [26]. This constrained the mass of the axion to  $6 \times 10^{-13} \lesssim m_A \lesssim 2.4 \times 10^4$  eV (calculated through the use of Equation 4). Section 5 considers the progression of astrophysical constraints, which now enforce the limit  $10^9 \lesssim f_A \lesssim 10^{12}$  GeV if inflation occurs after the PQ transition (see Section 3). The axion mass

arises from an anomaly coupling  $\theta G_{A\mu\nu}\tilde{G}_A^{\mu\nu}$  as a direct result of the  $U(1)_{PQ}$  symmetry having a chiral anomaly [17]. The mass is inversely proportional to  $f_A$ , as are axion couplings and lifetimes. If charge-carrying complex scalar fields can exist whilst neutral under electroweak interactions,  $f_A$  can be much greater than the electroweak scale. If not,  $f_A$  is associated with the breaking of electroweak interactions and axions would have masses in the keV range. These have already been ruled out experimentally [1]. The mass of the axion is of the form:

$$m_A = \frac{\sqrt{m_u m_d}}{m_u + m_d} m_\pi f_\pi \frac{1}{f_A}, \quad (3)$$

where  $m_\pi = 135$  MeV is the pion mass, the pion decay constant,  $m_u \simeq 4$  MeV,  $m_d \simeq 8$  MeV are the up and down quark masses, and  $f_\pi \simeq 93$  MeV is the pion decay constant. The axion mass is approximately [2, ?]:

$$m_A \simeq 6 \times 10^{-6} \text{ eV} \left( \frac{10^{12} \text{ GeV}}{f_A} \right). \quad (4)$$

#### 2.4.2 Axion-photon coupling

The axion-photon-photon coupling constant  $g_{A\gamma\gamma}$  is given by:

$$g_{A\gamma\gamma} = \frac{\alpha}{2\pi f_A} \left[ \frac{E}{N} \frac{2(4+z+w)}{4(1+z+w)} \right] = \frac{\alpha}{2\pi f_A} c_{A\gamma\gamma}, \quad (5)$$

where  $\alpha$  is the fine structure constant,  $z \equiv m_u/m_d$  and  $w \equiv m_u/m_s \ll z$  are quark-mass ratios and  $c_{A\gamma\gamma}$  is a coefficient assigned for ease [21].  $E/N$  is the ratio of the electromagnetic to colour anomalies of the Peccei-Quinn symmetry. This value is model dependent, with  $E/N = 8/3$  usually for DFSZ axions (though it depends on the charge assignment of leptons) and  $E/N = 0$  for KSVZ axions [27].

The interaction has a Lagrangian density, given by:

$$\mathcal{L} = -\frac{1}{4} g_{A\gamma\gamma} F^{\mu\nu} \tilde{F}_{\mu\nu} \phi_A, \quad (6)$$

where  $F_{\mu\nu}$  is the electromagnetic field tensor,  $\tilde{F}_{\mu\nu}$  its dual, and  $\phi_A$  the axion field [21].

#### 2.4.3 Axion-electron coupling

Axion-electron coupling can only occur in the DFSZ axion model at the tree-level, as no ordinary quarks, leptons or Higgs fields carry PQ charge [24]. The Lagrangian density for the axion-electron interaction is:

$$\mathcal{L} = i g_{Ae} \bar{\phi}_e \gamma_5 \phi_e \psi_A \quad (7)$$

where  $g_{Ae}$  is the dimensionless axion-electron coupling constant, which is again model dependent,  $\phi_e$  is the electron field,  $\psi_A$  is the axion isospin doublet, and  $\gamma_5$  is the Dirac gamma matrix

[21]. This coupling is beneficial to research due to the ability to induce the axio-electric effect. The axio-electric effect is analogous to the photoelectric effect, with the incident photon being replaced by an axion. There are three variants of the axio-electric effect that will be examined in this review: the Primakoff process, the Compton-like process, and bremsstrahlung.

#### 2.4.4 Axion-nucleon coupling

There are two possible contributions towards axion-nucleon coupling. Firstly, there is the tree-level coupling of the axion to up and down quarks. Secondly, there is a contribution due to the generic axion-pion mixing. This is due to the axion-gluon coupling, and the fact that axions and pions are bosons with the same quantum numbers. This means that even though the KSVZ axion does not couple directly to ordinary quarks, it has a coupling to nucleons [23].

The Lagrangian density is given by:

$$\mathcal{L} = i\bar{\psi}_N \gamma_5 (g_{AN}^0 + g_{AN}^3 \tau_3) \psi_N \phi_A \quad (8)$$

where  $\psi_N$  is the nucleon isospin doublet,  $\tau_3$  the associated isospin Pauli matrix, and  $\phi_A$  is the axion field [21]. The two dimensionless parameters  $g_{AN}^0$  and  $g_{AN}^3$  are the model-dependent isoscalar and isovector axion-nucleon coupling constants respectively.

## 2.5 ALPs

ALPs are pseudoscalars that do not necessarily solve the strong CP problem. These can also be considered dark matter candidates. ALPs can be produced in the same manner as axions, and are of particular interest in relation to the evolution of stars (see Section 5). This would indicate a coupling strength that would be detectable in the next generation of helioscope and laboratory experiments (see Section 7).

ALPs are motivated by string theory [29], which motivates the existence of this extension to the SM. Unlike the axion, the mass and couplings of ALPs are disproportionate, and are not directly related to their PQ-like scale [28]. Due to this, one would search for ALP couplings in a model-independent way, and in a much wider parameter window [21].

Figure 3 displays the parameter space available for ALPs. The subset of parameter space in which axions can be a solution to the strong CP problem is shown to be relatively small.

## 3 Axions as candidates for dark matter

If an axion or ALP is an NGB – i.e. if non-perturbative effects or symmetry breaking causes them to have a relatively small mass – their coupling to matter is predicted to be less than the

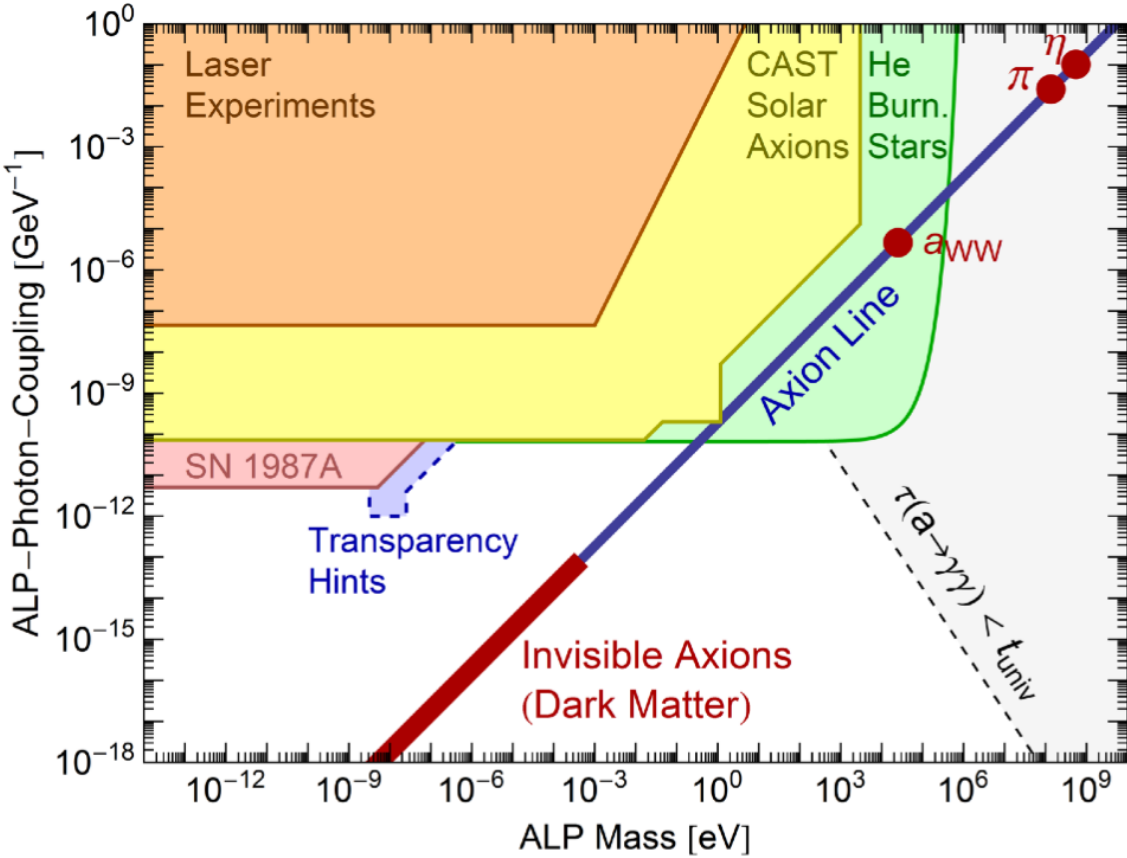


Figure 3: A graph of ALP mass (eV) vs. ALP photon coupling ( $\text{GeV}^{-1}$ ) displaying the parameter space for ALPs [30]. The constrained axionic parameter space is displayed as the dark blue line, with invisible axions constrained further to the red line.

weak interaction coupling strength, which in turn allows them to be regarded as a viable dark matter candidate. A large fraction of our universe is composed of dark matter. This can be explained by the dynamics of our galaxy if a non-relativistic dark matter halo exists that has a solar neighbourhood density of  $\rho_{\text{DM}} = 0.3 \text{ GeV/cm}^3$  [21]. Within the SM there are no viable candidates for dark matter, however, there are many candidates that could exist beyond the SM. Figure 4 displays the extent of possible dark matter contenders.

There are two basic constraints on dark matter candidates: that they must be stable for a time period longer than the age of the universe, and that they must be very weakly interacting (or non-interacting) cold dark matter. The latter means that they must be effectively collisionless, have a negligible primordial velocity distribution, and must have been produced in the early universe.



Figure 4: An *incomplete* graphical representation of the landscape of dark matter candidates due to T. Tait, from Reference [31]. Note the overlapping of ALPs and warm dark matter.

Due to the coupling of axions to photons, the axion decay rate would be

$$\Gamma = \frac{g_{A\gamma\gamma}^2 m_A^3}{64\pi} = \frac{\alpha^2}{256\pi^3} c_{A\gamma\gamma}^2 \frac{m_A^3}{f_A^2}, \quad (9)$$

where all of these variables are defined following Equation 5. Evaluating this, one finds the approximate decay rate of

$$\Gamma \simeq 2.2 \times 10^{-51} \text{sec}^{-1} \left( \frac{10^{12} \text{GeV}}{f_A} \right)^5. \quad (10)$$

Here the lifetime of the axion exceeds the age of the universe when  $f_A \gtrsim 10^5 \text{ GeV}$ . This shows that the invisible axion is nearly stable, which means that they have the ability to contribute to the formation of the cosmological structures observed in the universe today. Astrophysical constraints are shown to limit  $f_A$  further in Section 5, but it should be noted that axions also need to have a mass  $m_A \lesssim 20 \text{ eV}$  to exceed the age of the universe [?]. This is a cosmological constraint that must be imposed on axions for them to be viable dark matter candidates.

The other prerequisite is satisfied by the fact that axionic dark matter is non-relativistic despite its small predicted mass [32].

It is possible for axions to be produced in thermal production methods, however, there are issues preventing these axions from contributing to the bulk of dark matter in the universe. Firstly, axions would have a mass  $\sim 80 \text{ eV}$ , implying a short cosmic lifetime, shorter than the age of the universe [?]. It is thought that a sufficiently large quantity of non-relativistic axions exist to provide the required dark matter energy density of the universe, however, a mass this high would remove axions from the possible candidates that contribute to the bulk of the dark matter [33]. These axions are also excluded as they would have converted into photons that would have already been observed. Secondly, axions would be hot dark matter, breaking one of the basic constraints to be dark matter.

### 3.1 Cold Dark Matter Axion Production Mechanisms

Examining the axions that are produced in cold populations, there are three possible production mechanisms of axions that originate from topological defects: vacuum realignment, string decay, and domain wall decay. The likelihood of each of these production mechanisms depends on whether the PQ phase transition (where the axions are produced) and the QCD phase transition (where they acquire mass) occur before or after inflation. Inflation is the stage at which our universe is exponentially expanding, and if it occurs after the PQ phase transition, the cosmic density of the topological defects can be ignored. In this case, the isocurvature fluctuations of the axion field significantly constrain the axion models as they make an imprint on the anisotropies

of the Cosmic Microwave Background (CMB) [34]. Figure 5 displays the differences in  $m_A$  and  $f_A$  for the different cold dark matter scenarios.

When inflation occurs after the PQ transition, there is axion field homogenisation. This means that the axion field will have one value over the visible universe. Non-perturbative QCD effects cause a potential in the axion field, which, when significant, will cause the field to oscillate. These oscillations of the axion field do not decay over time, so ‘vacuum realignment’ causes a cold axion population [18, 19, 20], and a relic density of

$$\Omega_A \simeq 0.4 \theta_i^2 \left( \frac{f_A}{10^{12} \text{ GeV}} \right)^{1.18} \quad (11)$$

where  $\theta_i$  is the initial angle perturbation of the vacuum misalignment [?]. This evolution is called the ‘zero momentum mode’ [34]. For inflation to occur after the PQ phase transition one needs a sufficiently large value of  $f_A$ , which is bounded by the relic density of axions.

The axion density should not exceed the matter density of the present universe  $\Omega_{\text{CDM}} \simeq 0.227 \pm 0.014$  [?], so  $\Omega_a \leq \Omega_{\text{CDM}}$ , obtaining the upper bound of  $f_A \lesssim 10^{12} \text{ GeV}$  [?]. This bound does however have large uncertainties due to various cosmological scenarios.

If, for example, inflation occurs *before* the PQ phase transition, and  $f_A$  is smaller than required, the axion field would be inhomogeneous, and the aforementioned topological effects could have observable consequences.

In summary, cold dark matter axions are constrained as  $f_A \lesssim 10^{12} \text{ GeV} \theta_i^{-2}$ , for  $m_A \geq 10^{-6} \text{ eV} \theta_i^{-2}$  [?]. The  $\theta_i$  term accounts for the order of cosmic evolution, and is taken to be an arbitrary constant less than 1. If inflation occurs before the PQ transition then  $\theta_i \sim 1$ , however if it occurs after, the lower bound  $m_A \geq 10^{-6} \text{ eV} \theta_i^{-2}$  could be altered significantly by  $\theta_i \ll 1$ , dark matter could consist of axions entirely, and  $f_A$  could reach a value of  $10^{16} \text{ GeV}$ , near the grand unification energy [?]. Current estimates of the minimum fraction of dark matter that is made of axions is 37% [35].

### 3.2 Axions as a Bose-Einstein Condensate

There is an argument that axions contribute to the dark matter population of the universe due to their ability to form a rethermalising Bose-Einstein condensate (BEC). A BEC state occurs if identical bosonic particles are highly condensed in a phase space and if these particles thermalise (go to thermal equilibrium). Axions are extremely condensed in phase space, and are identical bosonic particles, but it was originally questioned whether they could thermalise.

It was originally thought that the axion coupling was so weak that BEC formation was highly unlikely. However, it was shown in Reference [36] that due to gravitational interactions they do have the ability to thermalise, and do so after a relaxation time  $\tau$ . N. Banik and P. Sikivie

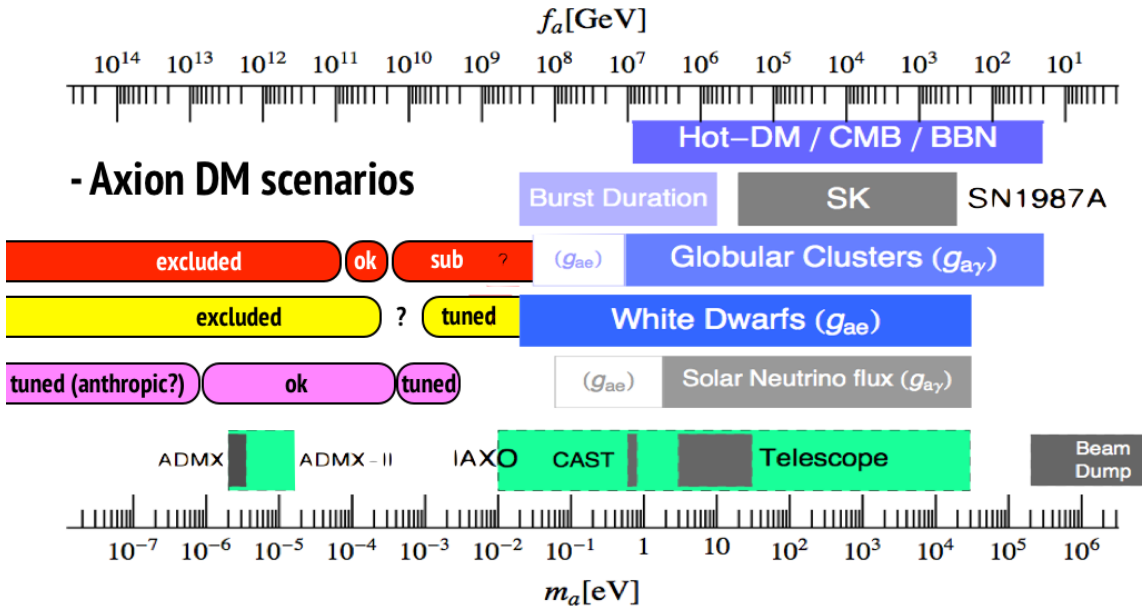


Figure 5: A diagram of the axion mass limits in the main cold dark matter scenarios for  $m_A$  (eV) and  $f_A$  (GeV) [22]. The constraints after inflation are shown in red and yellow. Cosmological, astrophysical and experimental bounds are shown, together with sensitivities from ADMX-II and IAXO (green).

(2009) found a relaxation time in the order of  $10^5$  years, which is much shorter than the age of the universe [37]. This means that axions would have been in a BEC state for a long period of time already. Usually particle gravitational interactions are negligible, but dark matter axions are a special case due to their ability to form a BEC and have a high occupation in a small number of states (typically  $10^{61}$  per quantum state) [37].

In addition, the caustic ring model of dark matter in galactic halos [38], and the existence of axions as a BEC could be the explanation behind this phenomenon [39]. This self-gravitating isothermal sphere model is the most widely used model of the galactic halo, yet it could fail as soon as angular momentum is introduced [37]. Axionic Bose-Einstein condensation was shown to provide a solution to this problem [37].

## 4 Astrophysical sources of axions and ALPs

Beyond dark matter, a promising avenue for observing axions or ALPs is via their production in stellar processes. Axions and ALPs can be produced in six stellar processes: bremsstrahlung, Primakoff production, Compton-like scattering, axio-recombination, axio-deexcitation [40] (variations of which are displayed in Figure 6), and the nuclear magnetic transition of  $^{57}\text{Fe}$  nuclei.

The relative intensity of the fluxes of these mechanisms are model dependent. For the DFSZ

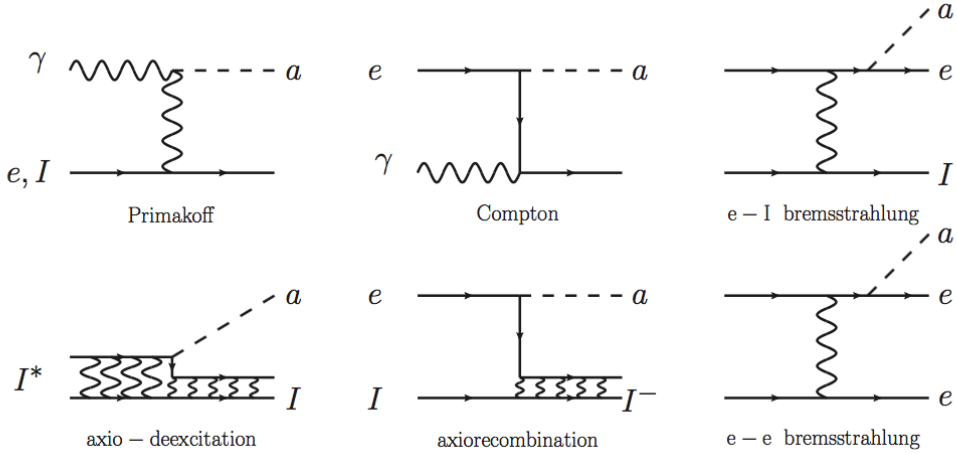


Figure 6: Feynman diagrams of non-hadronic axion model reactions responsible for solar axion flux [40].

axions the dominant processes in low mass stars, such as white dwarf (WD), main sequence (MS), and horizontal branch (HB) stars, are Compton-like and bremsstrahlung processes. In very low mass stars, axio-recombinations are also prevalent processes. For KSVZ axions, the Primakoff effect dominates. The EDELWEISS collaboration calculated the fluxes at Earth for each of these processes; the result is shown in Figure 7. Assuming that axions constitute all of dark matter, the average expected flux at Earth of the sum of the possible mechanisms is:

$$\Phi_{\text{DM}} (\text{cm}^{-2} \text{s}^{-1}) = \rho_{\text{DM}} \cdot \frac{v_A}{m_A} = 9.0 \times 10^{15} \left( \frac{\text{keV}}{m_A} \right) \cdot \beta, \quad (12)$$

where the flux  $\Phi_{\text{DM}}$  is independent of axion coupling,  $m_A$  is the mass of the axion,  $\rho_{\text{DM}}$  as defined in Section 3,  $v_A$  is the mean axion velocity distribution with respect to the Earth, and  $\beta \simeq 10^{-3}$  [21].

The electron-positron annihilation,  $e^+ + e^- \rightarrow \gamma + A$ , is another possible axion production channel, but it is not a predominant mechanism. This is as far as this review will consider this process, as positrons are only present in large enough quantities at high temperatures. Bremsstrahlung and other processes become significantly more dominant at this point [26].

#### 4.1 Primakoff production

Thermal photons could be converted into axions in the presence of charged particles in a process called the Primakoff process:

$$e^- + \gamma \rightarrow e^- + A. \quad (13)$$

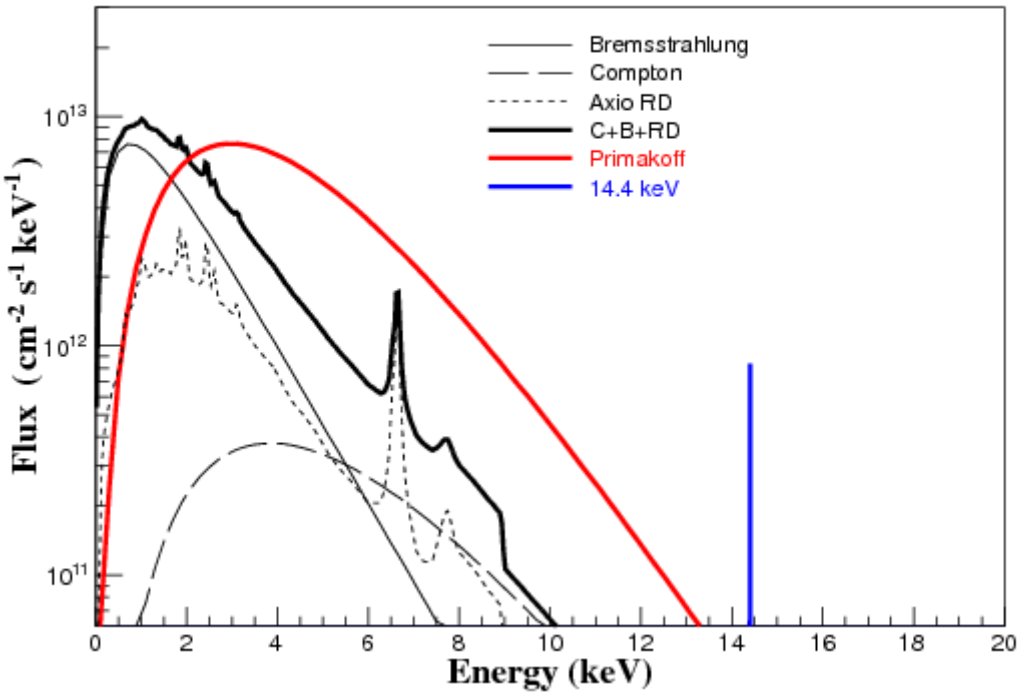


Figure 7: A graph displaying flux ( $\text{cm}^{-2}\text{s}^{-1}\text{keV}^{-1}$ ) vs. energy (keV) for the predicted solar axion fluxes on Earth from different mechanisms (in the EDELWEISS-II detectors) [21]. Axio-recombination and axio-deexcitation have been combined here to the axio-RD mechanism. The effective axion couplings represented here are  $g_{A\gamma} = 10^{-9} \text{ GeV}^{-1}$ ,  $g_{Ae} = 10^{-11} \text{ GeV}^{-1}$  and  $g_{AN}^{eff} = 10^{-7} \text{ GeV}^{-1}$ .

This process has the Lagrangian density as shown in Equation 5. Charged particles exist in the electromagnetic field of the plasma around a stellar object, so production in an object like the Sun could be extremely efficient. Primakoff production in degenerate plasma dominates the other production mechanisms as there are more free photons than charged particles. Therefore this is the mechanism predominantly considered in detection attempts of axions and ALPs [27].

The expected solar axion flux produced through the Primakoff process corresponds to a broad spectrum (visible in Figure 7). An exception, as is explained in Sections 4.2 and 4.3, is for the DFSZ models. The expected solar flux at Earth (in  $\text{cm}^{-2}\text{s}^{-1}\text{keV}^{-1}$ ) is approximated by the equation:

$$\frac{d\Phi}{dE} = \frac{6.02 \times 10^{14}}{\text{cm}^2\text{keV s}} \left( \frac{g_{A\gamma} \times 10^8}{\text{GeV}^{-1}} \right)^2 E^{2.481} e^{-E/1.205}, \quad (14)$$

where the energy  $E$  is in keV [21]. The coupling of the Primakoff process is limited by Equation 5.

The Primakoff production can be reversed so that an axion in an electromagnetic field

couples to a virtual photon and converts into a real photon [23]. This mechanism therefore allows detection of axions in laboratory experiments, particularly in the use of helioscopes, haloscopes, and crystal detectors (see Section 6).

## 4.2 Compton-like scattering

The Compton-like scattering process is the simplest possible mechanism to produce axions through their coupling to electrons. A photon scatters with an electron, causing the electron to recoil and an axion to be emitted:

$$e^- + \gamma \rightarrow e^- + A. \quad (15)$$

The energy of the photon is the same as the outgoing axion. The Lagrangian density for this process is the Lagrangian density for the axion-electron coupling shown in Equation 5. For DFSZ axions the axio-electric coupling is restricted to:

$$(g_{Ae})_{\text{DFSZ}} = \frac{m_e}{3f_A} \cos^2 \beta_{\text{DFSZ}} \simeq 1.68 \times 10^{-4} \frac{\text{GeV}}{f_A} \simeq 2.84 \times 10^{-8} \frac{m_A}{\text{keV}}, \quad (16)$$

where  $\cos \beta_{\text{DFSZ}} = 1$  for model dependent studies [21].

For KSVZ axions the axio-electric coupling is restricted to:

$$(g_{Ae})_{\text{KSVZ}} = \frac{3\alpha^2 N m_e}{2\pi f_A} \left( \frac{E}{N} \ln \frac{f_A}{m_e} - \frac{2}{3} \frac{4+z+w}{1+z+w} \ln \frac{\Lambda}{m_e} \right) \simeq -5.7 \times 10^{-7} \frac{\text{GeV}}{f_A}, \quad (17)$$

where  $\Lambda \sim 1 \text{ GeV}$  is associated with the QCD confinement scale [21].

This mechanism is particularly important in axion emission from the Sun and HB stars. The expected solar flux at Earth (in  $\text{cm}^{-2} \text{s}^{-1} \text{keV}^{-1}$ ) is approximated by the equation [21]:

$$\frac{d\Phi}{dE} = g_{Ae}^2 \times 1.33 \times 10^{33} E^{2.987} e^{-0.776E}. \quad (18)$$

The Compton-like effect corresponds to the transverse electromagnetic field, and is mostly dominated by other production mechanisms, particularly where axion emission occurs from a degenerate plasma [26]. In non-degenerate plasma, there are more charged particles than free photons, therefore the Compton-like effect competes with bremsstrahlung. For the same value of  $f_A$ , the flux for the DFSZ model is much higher than that of the KSVZ model. This is due to the tree-level coupling of axions to electrons (see Section 2.3.2). For the DFSZ model the Compton-like process dominates the Primakoff process [21].

## 4.3 Bremsstrahlung

The bremsstrahlung process occurs when electrons in the presence of charged particles emit an axion. In particular, a stellar plasma is an ideal environment for this to occur. It is also known

as the free-free electron transition, and is of the form:

$$e^- + I \rightarrow e^- + I + A, \quad (19)$$

where  $I$  is an ion. The Lagrangian density for this process comes from the axion-electron coupling as shown in Equation 5. The axio-electric coupling is bounded by the same equations as for the Compton-like effect (Equations 16 and 17). The expected solar flux at Earth (in  $\text{cm}^{-2} \text{s}^{-1} \text{keV}^{-1}$ ) is approximated by the equation [21]:

$$\frac{d\Phi}{dE} = g_{Ae}^2 \times 2.63 \times 10^{35} E e^{-0.77E} \frac{1}{1 + 0.667E^{1.278}}. \quad (20)$$

Just as for the Compton-like effect, and for the same reason, the flux for the DFSZ model is more intense than that of the KSVZ model.

Bremsstrahlung production mechanisms differ within degenerate and non-degenerate plasmas. In a degenerate plasma, bremsstrahlung is particularly efficient. This occurs in WDs and the cores of red giants before the helium flash. Here, Primakoff production and Compton-like processes are suppressed by a large plasma frequency [25]. In non-degenerate plasma, bremsstrahlung competes with the Compton-like effect. Bremsstrahlung emission corresponds to the longitudinal electromagnetic field [25].

#### 4.4 Axio-recombination and axio-deexcitation

Axio-deexcitation is deexcitation of a bound electron in an ion that is in an excited state. This process is also known as bound-bound electron transitions and is of the form:

$$I^* \rightarrow I + A. \quad (21)$$

where  $I^*$  is the excited state of ion  $I$  [21]. The Lagrangian density for this process originates from the axion-electron coupling.

Axio-recombination is the process in which a nucleus captures an electron to form an ion. This is electron capture, which is also known as free-bound electron transitions, and is of the form:

$$e^- + I \rightarrow I^- + A, \quad (22)$$

where  $I^-$  is the deexcited state of ion  $I$  [21]. The effect can be detected within crystal detectors, where the axio-electric effect can cause electron recoil. The Lagrangian density for this process is also chosen as the axion-electron coupling Lagrangian density.

## 4.5 Nuclear magnetic transition of $^{57}\text{Fe}$ nuclei

Due to the high temperatures in stellar objects, the de-excitation of the low energy levels of some nuclei could be another production mechanism of axions. In particular, the  $^{57}\text{Fe}$  isotope is a heavy, highly abundant and stable element present in solar objects. This could emit monochromatic axions of energy 14.4 keV from an M1 transition, in the form:



Crystal detectors can make use of this nuclear magnetic transition by measuring electron recoil. The corresponding axion flux at Earth is given by:

$$\Phi_{14.4} = \left( \frac{k_A}{k_\gamma} \right) \times 4.56 \times 10^{23} \left( g_{AN}^{\text{eff}} \right)^2 \text{ cm}^{-2}\text{s}^{-1}. \quad (24)$$

where the effective axion-nucleon coupling constant  $g_{AN}^{\text{eff}} \equiv (-1.19g_{AN}^0 + g_{AN}^3)$  [23], and  $\frac{k_A}{k_\gamma}$  is the ratio of the momenta of the outgoing axion and photon where, to take into account the non-relativistic limit, the ratio is not set equal to 1. The Lagrangian density is given by Equation 8, with model-dependent isoscalar and isovector axion-nucleon coupling constants. Evaluating these constants for KSVZ and DFSZ models give fluxes that are of the same order of magnitude, therefore the axion production rate for this process does not vary significantly for each model [41].

## 5 Constraints from astrophysics

This section considers the constraints on axion and ALP masses and couplings imposed by astrophysical and cosmological observations. It is shown that these limits enforce  $10^9 \lesssim f_A \lesssim 10^{12} \text{ GeV}$ . Using Equation 4, the axion mass is therefore constrained to  $10^{-6} \lesssim m_A \lesssim 10^{-3} \text{ eV}$ .

### 5.1 Stellar energy loss limits

As the emission of axions is a channel of energy loss, the rate at which stellar objects evolve and radiate energy allows us to place strict limits on their couplings and masses.

Firstly, if the Sun loses energy through axion emission, then to allow for this extra energy loss whilst respecting the age and brightness inferred from measurements, there needs to be enhanced nuclear burning. This would result in an increase in the solar neutrino flux [42]. The observation of this flux bounds  $g_{A\gamma\gamma} \lesssim 7 \times 10^{-10} \text{ GeV}^{-1}$  [43]. Secondly, through the observations of globular clusters a bound of  $g_{A\gamma\gamma} \lesssim 0.6 \times 10^{-10} \text{ GeV}^{-1}$  was derived from the helium-burning lifetimes of the HB stars [44]. Thirdly, WDs constrain the axion-electron coupling

to  $g_{Aee} \simeq (0.6 - 1.7) \times 10^{-13} \text{ GeV}^{-1}$  through the calculation of the radiation of energy in the form of axions to allow for theoretical cooling [45]. It was reported by J. Isern *et al.*(2008) that the luminosity function of WDs fits better when axion cooling is applied [46]. Fourthly, due to delay of helium ignition in red giant branch stars due to axion cooling, constraints were made of  $m_A \lesssim 9 \times 10^{-3}$ , or  $g_{Aee} \lesssim 2.5 \times 10^{-13} \text{ GeV}^{-1}$  [47]. Finally, axion emission could provide a major cooling mechanism for neutron stars, which gives an upper bound on the axion mass of  $m_A < 2 \times 10^{-2} \text{ eV}$ . This prevents theory predicting that they cool down faster than observation implies [48].

These coupling constraints imply model-dependent constraints on the axion scale parameter  $f_A$ . However, for ALPs, or other models beyond DFSZ and KSVZ the relation between  $f_A$  and mass are independent. This explains the large ALP parameter space, as shown in Figure 3, which exhibits an ALP mass range of up to 1 GeV.

## 5.2 X-ray satellite

A satellite could be used to observe axions and ALPs that have converted from X-ray photons via the bremsstrahlung and Compton-like processes in the Earth's magnetic field. The sensitivity to  $g_{A\gamma\gamma}$  could be comparable to CAST, but only for much smaller  $m_A$  [49].

The X-ray Multi Mirror satellite (XMM-Newton) [50] observed a seasonally varying X-ray background signal. Discounting other known sources of X-rays this signal strength should be independent of the satellite position, however, a slightly more intense X-ray signal was detected on the side of the Earth closest to the Sun than the side that is farthest. Fraser *et al.* report that this variation in the signal is consistent with the conversion of solar axions in the Earth's magnetic field. A limit for the product of the axion-electron and axion-photon coupling constants was derived to be  $g_{Aee}g_{A\gamma\gamma} \sim 2.2 \times 10^{-22} \text{ GeV}^{-1}$  for an axion mass  $m_A \sim 10^{-3} \text{ eV}$  [50]. NASA's Chandra X-Ray Observatory could produce synonymous results, though the apparatus sensitivity is significantly lower due to a very high angular resolution. Therefore more data and analysis is needed to produce conclusive results. In addition, the XMM-Newton results are inconsistent with WD and neutron star cooling, which infer an axion mass  $m_A \sim 10^{-2} \text{ eV}$ . Currently, therefore, due to the discrepancy with astrophysical constraints, these results are still speculative.

## 5.3 Conversion of astrophysical photon fluxes

In large scale magnetic fields axion-photon oscillations can be initiated due to the astronomical distances involved. The photon flux is measured by an instrument such as a telescope, and the results are compared with theory. A discrepancy between measurement and prediction can be modelled by introducing axion-photon coupling. Observations which are consistent with the

predicted fluxes can therefore be used to set limits on the size of the axion-photon coupling. Similarly, the axion-photon coupling can introduce a change in the polarisation of the photon flux, and so an analogous search can be made via measuring the polarisation instead of the photon beam intensity from a source.

Due to Primakoff production, the supernova (SN) 1987A could have emitted ALPs which would have partially converted into gamma rays as they travelled through its magnetic field. However there were no gamma rays detected, providing a limit of  $g_{A\gamma\gamma} \lesssim 1 \times 10^{-11} \text{ GeV}^{-1}$  for  $m_A \lesssim 10^{-9} \text{ eV}$  [51]. The SN 1987A gave a lower bound for the KSVZ axion scale parameter of  $f_A \geq 4 \times 10^8 \text{ GeV}$  [52]. Frequency dependent dimming caused by the ALP photon oscillations in the magnetic field could have influenced the estimation of cosmic acceleration that used Type 1a supernovae. However, Mirizzi *et al.* claim that photon-axion oscillations do not have a significant effect on Type 1a supernovae dimming due to the examination of the Cosmic Microwave Background (CMB) excluding a previously allowed parameter region [53].

The non-observation of the modification of polarisation due to photon fluxes from magnetic WDs give ALP limits close to  $g_{A\gamma\gamma} \lesssim 10^{-8} \text{ GeV}^{-1}$  for  $m_A \lesssim 10^{-5} \text{ eV}$ , and  $g_{A\gamma\gamma} \lesssim 10^{-11} \text{ GeV}^{-1}$  for  $m_A \lesssim 10^{-7} \text{ eV}$  [54]. This research only searched in the range  $m_A \leq 10^{-5} \text{ eV}$  as higher masses do not constrain  $g_{A\gamma\gamma}$  better than HB stars and CAST limits. In Figure 8 the axion mass has been constrained to  $10^{-6} \text{ eV} \lesssim m_A \lesssim 10^{-2} \text{ eV}$  from existing cosmological and astrophysical constraints, and capped at  $g_{A\gamma\gamma} < 10^{-10} \text{ GeV}^{-1}$  from HB star limits, meaning the constraints given by magnetic WDs are outside of the axion parameter space, but still constrain ALPs.

The Fermi-LAT telescope searched for spectral irregularities induced by photon-ALP oscillations from the central galaxy of the Perseus cluster. The irregularities were not observed, therefore ALP couplings were limited to  $g_A < 5 \times 10^{-12} \text{ GeV}^{-1}$  for ALP masses  $0.5 \times 10^{-9} \lesssim m_A \lesssim 5 \times 10^{-9} \text{ eV}$  at 95% confidence [28].

## 6 Laboratory searches for axions and ALPs

This section reviews the searches for axions and ALPs via direct detection. The experimental methods that are investigated in this section are: photon regeneration, birefringence and dichroism, helioscopes, haloscopes and Bragg diffraction scattering.

### 6.1 Photon regeneration

Photon regeneration experiments are also known as the ‘light shining through wall’ (LSW) experiments [55]. Optical photons, X-rays and microwaves propagating through a transverse magnetic field could convert into ALPs, then back again, via the Primakoff production mechanism

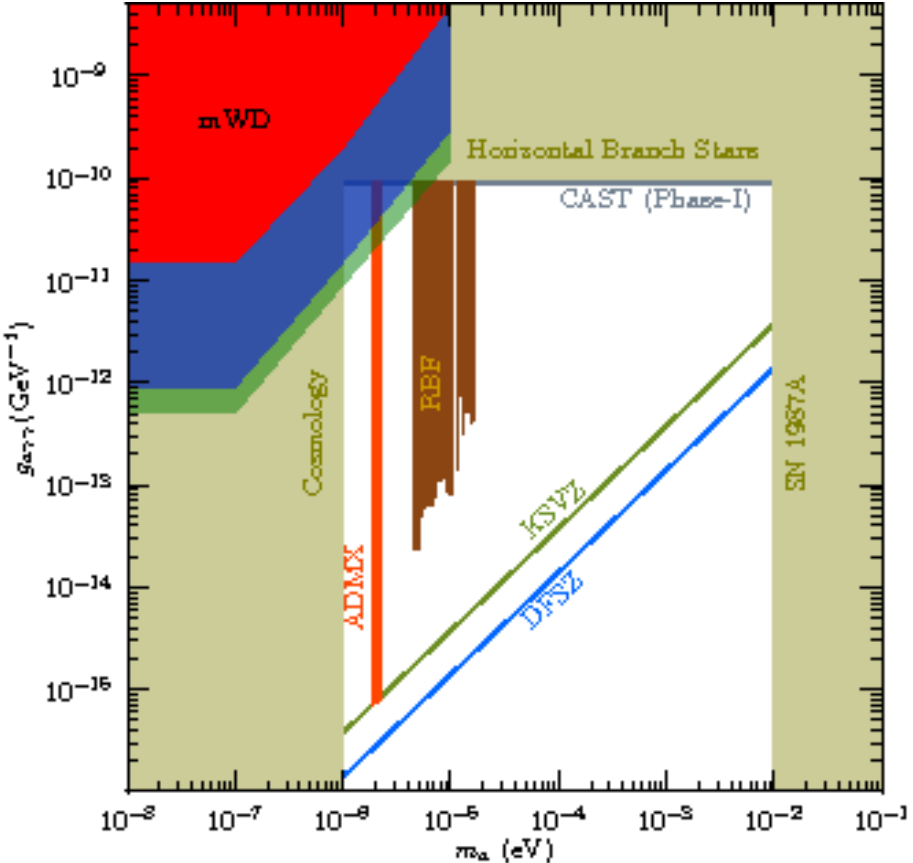


Figure 8: An exclusion graph of  $g_{A\gamma\gamma}$  ( $\text{GeV}^{-1}$ ) vs.  $m_A$  (eV) [54]. The red section is the constraint placed by magnetic WDs (magnetic field strength  $B \simeq 10^8 \text{ GeV}$ ), with the blue and dark green regions corresponding to  $B \simeq 10^9 \text{ GeV}$  and varying degrees of polarisation.

(see Section 4.1). Figure 9 shows the LSW experiment schematic. A magnetic field provides the virtual photons needed for this production mechanism. In this experiment a photon signal is propagated towards an optically shielded (photon-absorbing) wall, so only the photons that have converted into ALPs can pass through it. The photons can be then be regenerated with the same characteristics as the original photons using a second magnet that is in line with the original magnet [56].

The Any-Light-Particle-Search (ALPS) experiment [57] is a current LSW experiment that has produced interesting results. It searches for any Weakly Interacting Sub-eV Particles (WISPs), and uses a laser system to generate the primary photon beam and search for a signal of axion-induced photon regeneration, as shown in Figure 10. This beam is directed into a vacuum pipe, where an optical resonator is used to increase the laser power, enhancing proportionally any WISP (or axion) flux. Here the magnet used is a superconducting dipole magnet, which provides an 8.8 m magnetic field of 5 T. At the end of this regeneration tube, there is a light-tight box in which the beam is directed into a lens by a mirror, which then focuses the beam onto a  $\approx 30 \mu\text{m}$

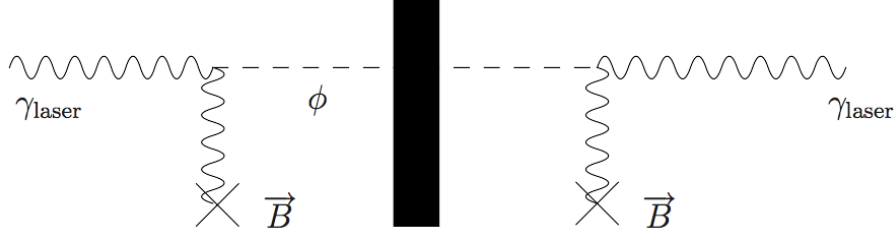


Figure 9: The schematic for a LSW experiment [58]. The photons from the laser convert to axions, travel through the optical wall, then convert back into photons, due to the magnetic field  $\vec{B}$ .

diameter beam spot on a CCD camera (which has undergone a series of upgrades to reduce noise and improve the quantum efficiency). The total beam intensity is measured by CCD pixels. The analog-to-digital unit (ADU) values of the signal pixel are compared with those of a reference beam ( $1 \text{ ADU} \equiv 1e^-$ ), and the footprint of the LSW is searched for.

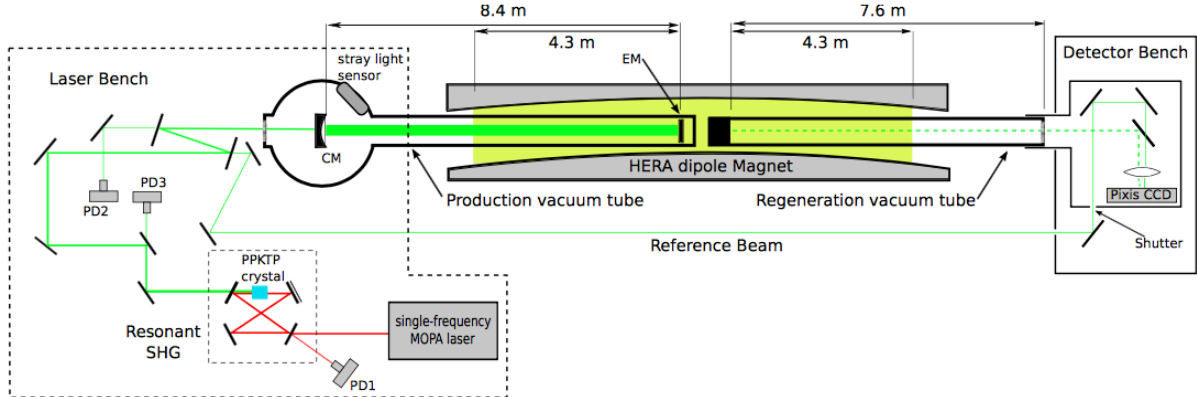


Figure 10: The schematic for the ALPS LSW experiment [57]. The beam is split into the main beam and the reference beam, before the main beam enters the vacuum tube. The two beams are then compared to search for ALPs.

ALPS constrained the axion-photon coupling via no detection of a change in the photon flux through the regeneration tube with respect to the primary laser flux. The constraint was published as  $g_{A\gamma\gamma} < 0.7 \times 10^{-7} \text{ GeV}^{-1}$  at 95% CL for  $m_A \lesssim 0.5 \times 10^{-3}$  [57], with Figure 11 displaying their ALP parameter space constraints.

## 6.2 Birefringence and Dichroism

An alternate method to search for axions is to measure the polarisation of a beam of photons. The beam polarisation changes if a photon in the beam converts to an axion. This occurs because the polarisation of the beam is modified as it propagates through a transverse magnetic field.

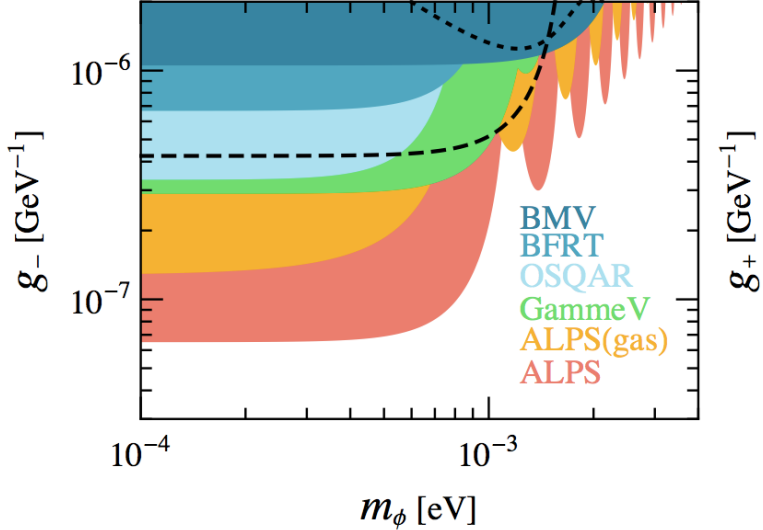


Figure 11: An exclusion graph of  $g_- (\text{GeV}^{-1})$  vs.  $m_A$  (eV) for the ALPS experiment parameter space. The red limit is from the ALP vacuum run [57].

The polarisation of the beam is subject to certain effects as it propagates through a transverse magnetic field. One of the effects that influence the polarisation is ‘dichroism’. This is where the parallel component of energy of the beam is depleted by axion production, but the perpendicular component is not. A slight rotation is therefore created in the linearly polarised beam [59]. Another effect which affects the energy components in a similar way is ‘birefringence’. The polarised beam again rotates, however, this time it rotates due to a mixing of virtual axions in the parallel energy state [59]. As a consequence the linearly polarised light develops an elliptical polarisation. These two effects are displayed in Figure 12.

The two effects can be searched for separately. An early experiment used dipole magnets to find that the dichroic rotation gave a stronger limit than birefringence, with  $g_{A\gamma\gamma} < 3.6 \times 10^{-7} \text{ GeV}^{-1}$  at 95% CL for  $m_A < 5 \times 10^{-4} \text{ eV}$  [60]. The birefringence limits are better at heavier axion masses as the dichroism effects vanish when  $m_A > E_\gamma$ , where  $E_\gamma$  is the energy of the converting photon.

The Polarizzazione del Vuoto con LASer (PVLAS - translated as “polarisation of the vacuum with laser”) experiment employs this detection method. Figure 13 displays the schematic of the apparatus, which is oriented in the vertical direction, and a detailed description and method can be found in Reference [58]. In summary, it consists of a 1 m long magnetic field in a vacuum produced by a 5.5 T rotating dipole magnet, and a highly sensitive ellipsometer that would be able to detect the small variations in the polarisation state of the light propagating through. The light that is transmitted through the crossed polariser P2 is detected by a photodiode. If an ellipticity or rotation is induced by either effect, an electric field component perpendicular to

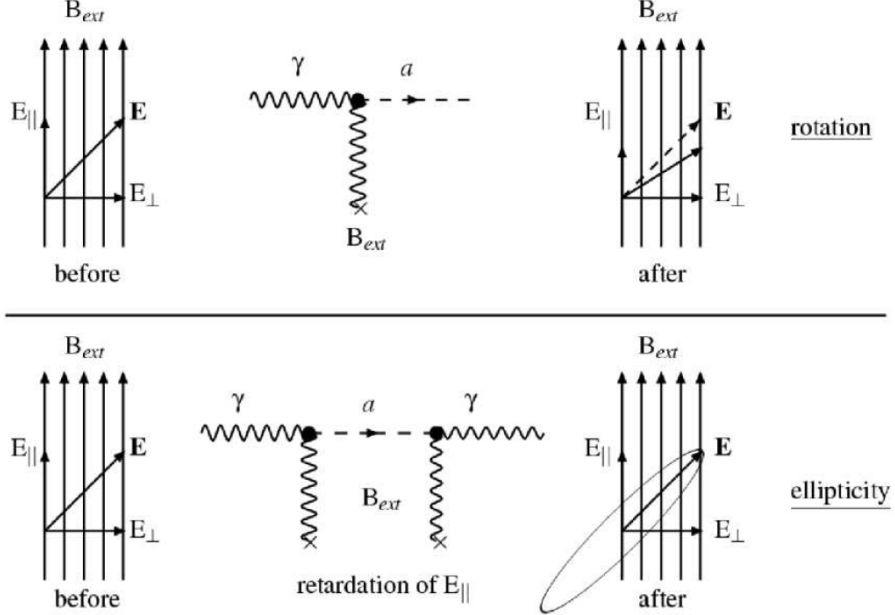


Figure 12: Diagrams displaying the effects of dichroism (top) and birefringence (bottom). Dichroism causes a rotation of the linear beam, whereas birefringence causes ellipticity [17].

the original polarisation may be generated within the cavity. There is a phase difference in the electric field of  $\pi/2$  between ellipticity and rotation, which makes the two effects distinguishable. The magnetic field causes vacuum birefringence, but the desired measurement would be the masking of this due to the existence of a light pseudoscalar particle, such as an axion.

The PVLAS collaboration reported a dichroism signature that was interpreted as a possible ALP with  $1 \leq m_A \leq 1.5 \times 10^{-3} \text{ eV}$  and  $1.6 \leq g_{A\gamma\gamma} \leq 5 \times 10^{-6} \text{ GeV}^{-1}$  [61]. However this report was subsequently excluded by the LSW experimental results, and was also attributed to ‘instrumental artifacts’ [62].

PVLAS published new constraints due to the non-observation of ellipticity or rotation in new data [62]. Figure 14 shows these limits.

### 6.3 Helioscopes

Helioscopes are experiments that search for axions that have been produced in the Sun using long dipole magnets oriented in the direction of the Sun. An axion that has been produced by the Primakoff process in the Sun (see Section 4.1) can convert to a photon in the dipole magnetic field [23, 63]. This photon would be in the X-ray range, would have the same energy as the axion, and could be detected in an X-ray detector at the end of the field, as displayed in Figure 15. So far, no evidence for axion-photon coupling has been observed in Helioscopes, resulting in limits on the axion-photon coupling and mass.

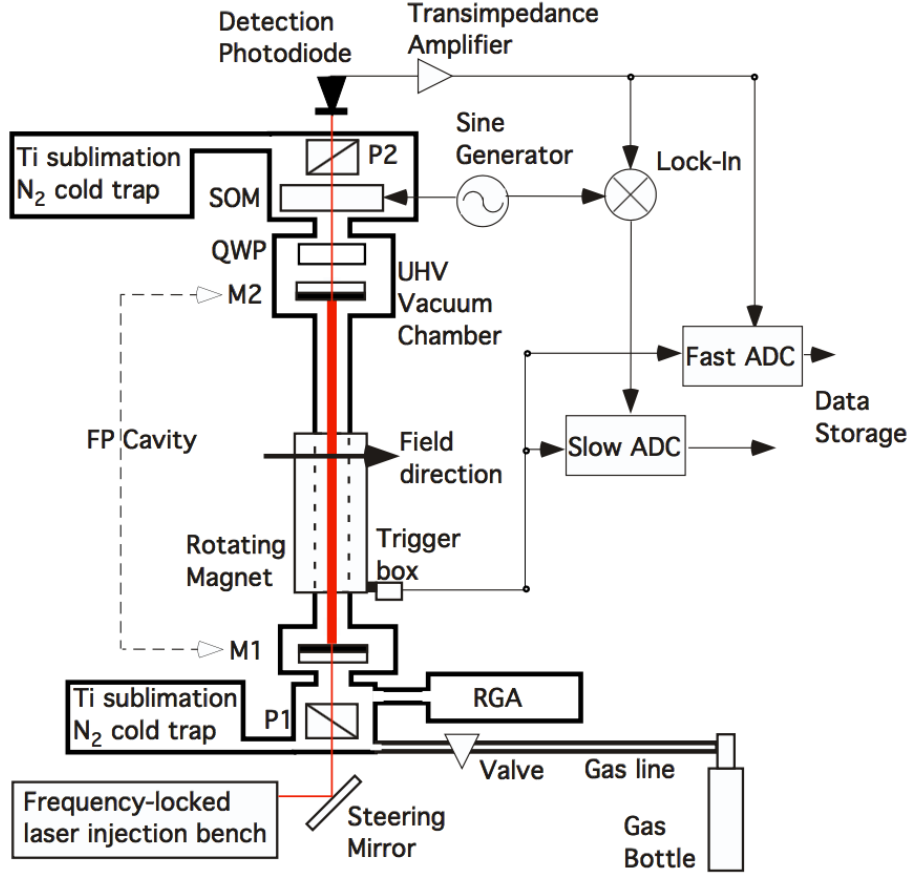


Figure 13: The schematic of PVLAS, which is oriented in the vertical direction [58]. Simplified, the beam is injected, traverses through the cavity immersed in a magnetic field, detected at a photodiode, amplified and analysed.

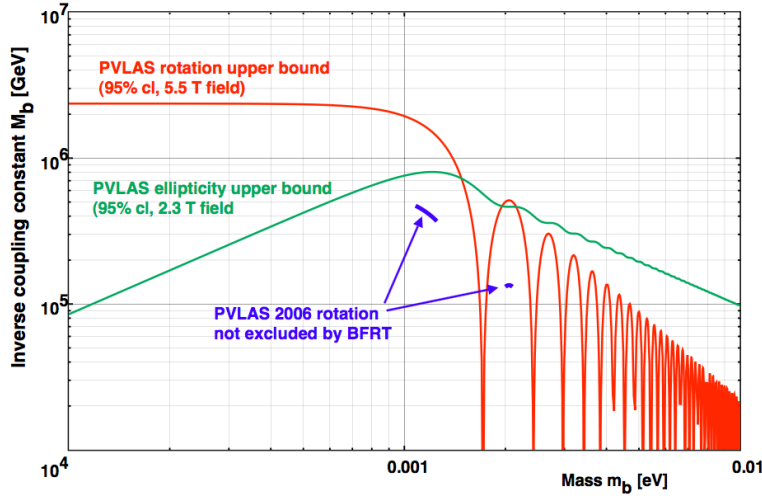


Figure 14: A graph of the PVLAS results, with inverse coupling constant  $M_b$  (GeV) vs. mass  $m_b$  (eV) for scalar or pseudoscalar bosons coupled to two photons [62].

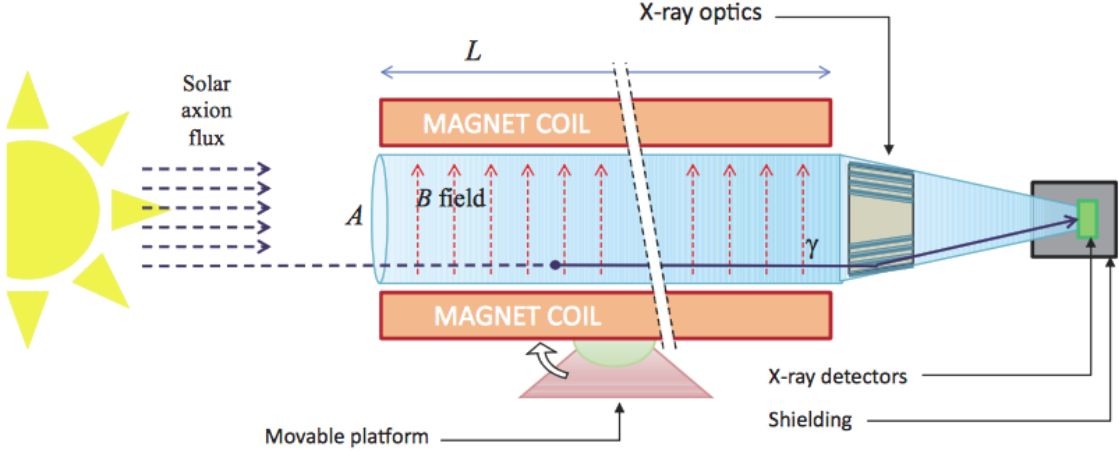


Figure 15: A general schematic of a helioscope [64]. The axions convert to photons – via the reverse Primakoff effect – within the magnetic field  $\vec{B}$ . The photons are focused on an X-ray detector and the signal is analysed.

Originally a conventional dipole magnet was used discontinuously (for only 1000 s/day) at the Brookhaven National Laboratory, and axions were excluded for  $g_{A\gamma\gamma} < 3.6 \times 10^{-9} \text{ GeV}^{-1}$  for  $m_A < 0.03 \text{ eV}$ , and  $g_{A\gamma\gamma} < 7.7 \times 10^{-9} \text{ GeV}^{-1}$  for  $0.03 < m_A < 0.11 \text{ eV}$  at 95% CL [65].

Later, the Tokyo Axion Helioscope used a superconducting magnet placed on a mount that rotated such that it tracked the Sun. After continuously taking data, a coupling of  $g_{A\gamma\gamma} < 6 \times 10^{-10} \text{ GeV}^{-1}$  was constrained for an axion mass  $m_A < 0.3 \text{ eV}$ . This experiment was then recommissioned and a similar limit was found of  $5.6 \times 10^{-10} \leq g_{A\gamma\gamma} \leq 13.4 \times 10^{-10} \text{ GeV}^{-1}$  in the mass region  $0.84 < m_A < 1.00 \text{ eV}$  [66, 67].

The most recent helioscope is the CERN Axion Solar Telescope (CAST), which searches for solar axions coupling to matter through the axion-photon coupling [23]. This apparatus uses a decommissioned LHC dipole magnet on a tracking mount. Four X-ray detectors are mounted on each side of the magnet, and the magnet is cooled to make it cryogenic. Phase I of CAST established the bounds  $g_{A\gamma\gamma} < 8.8 \times 10^{-11} \text{ GeV}^{-1}$  for  $m_A < 0.02 \text{ eV}$  with a 95% CL. [27]. Phase II of the experiment filled the conversion region with a buffer gas due to the cryogenic nature of the magnet to improve sensitivity. Helium-4 was used at varying pressure to search through the mass range  $m_A < 0.4 \text{ (eV)}$ , then helium-3 was used to achieve a higher pressure and therefore search at larger masses. Recent results were published with the bounds  $g_{A\gamma\gamma} < 8.8 \times 10^{-11} \text{ GeV}^{-1}$  at 95% CL for  $m_A < 0.02 \text{ eV}/c^2$  [68]. As displayed in Figure 16, CAST managed to cross the KSVZ axion line.

The next generation of helioscope searches could improve this bound by another order of magnitude. This is discussed in Section 7.2.



Figure 16: A graph of  $g_{A\gamma}$  (Gev $^{-1}$ ) vs.  $m_A$  (eV) at a 95% CL for CAST Phase I and II results [68]. The theoretical QCD axion models (yellow band) and the KSVZ model with  $E/N = 0$  (green) are displayed for comparison.

## 6.4 Haloscopes

Axions and ALPs could contribute to a large fraction of dark matter and therefore be detected through the investigation of the galactic halo. Haloscopes search for the axions that may be present in the halo.

### 6.4.1 The Microwave Cavity Haloscope

In 1983 Sikivie proposed [69] the haloscope detection method, to search for axions present in the galactic dark matter halo. Through the proposed use of a microwave cavity, Sikivie showed that these axions could convert into a resonant, monochromatic microwave signal when passing through a strong magnetic field. The condition for the conversion of axions to the microwave signal is that the cavity frequency must equal the axion mass. The search for the signal is performed through the tuning of the cavity frequency in very small, overlapping steps. However the signal is expected to be of the order of  $10^{-22}$  W, which creates a problem with detecting it over the noise of the system [70].

This type of haloscope consists of a cavity, a magnet and an antenna. The cavity has a high quality factor Q (a measure of efficiency), and is permeated by a strong magnetic field  $\vec{B}$  created by the magnet. Figure 17 shows the general setup of a microwave cavity and the processing of the signal.

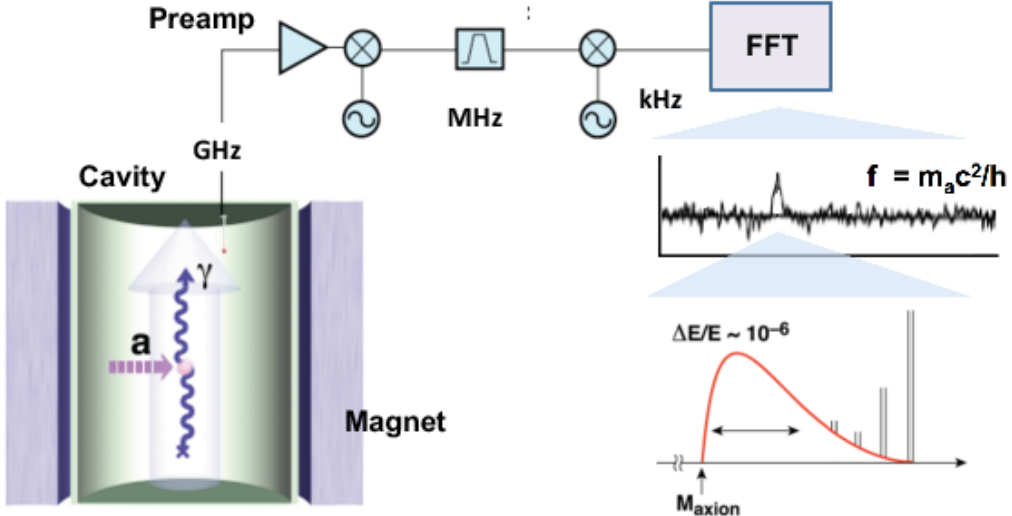


Figure 17: A diagram of a resonant microwave cavity detector [71]. Axions resonantly convert to a microwave signal cavity permeated by a strong magnetic field; the signal is extracted from the cavity by an antenna, amplified, mixed down, and then the power spectrum is calculated by a FFT. The associated signal expected from axion-photon conversions is displayed.

When the axion converts into a microwave photon, an antenna extracts the resulting signal from the microwave cavity and amplifies it. The signal represents the detection of the axion and contains the information of its instantaneous energy. The power spectrum of the signal is then calculated using a fast Fourier transform (FFT) after it has been mixed down into the audio signal range [72]. In addition to detection, if the axion has a fine structure on top of its own spectrum, more information could be obtained about the velocity dispersion of the axions in the dark matter halo, which is sensitive to the formation history of the galaxy. Due to the motion of the Earth through the dark matter halo, the frequency of the fine structure would show modulations due to the Earth's orbital and rotational velocities [73].

After the publication of the microwave cavity proposal, a few early experiments paved the way in cavity design [74, 75]. These prototypes, however, did not have the sensitivity to observe PQ axions over the system noise due to restrictions in amplifier technology.

Later, in 1995, the ADMX collaboration designed the Axion Dark Matter eXperiment (ADMX) to search for KSVZ galactic halo axions [76]. Here, the cavity volume was scaled up

from the earlier experiments by two orders of magnitude. In addition to this, the amplifier technology had improved enough to benefit the axion search.

The key technology that gives the experiment its sensitivity is the use of low-noise microwave amplification. This improves both the sensitivity and the frequency scanning rate of the experiment. The most recent phase of ADMX uses DC superconducting quantum interference device (SQUID) microwave amplifiers. When cooled with a dilution refrigerator, these will have noise temperatures approaching the quantum limit [70]. Section 7.3 discusses the addition of the dilution refrigerator to ADMX as a part of its ongoing upgrade. This means the system has a noise of  $\sim 50$  mK at signal frequencies near 1 GHz. Figure 18, shows the ADMX experiment setup, with the SQUID amplifier and the magnet with microwave cavity inside.

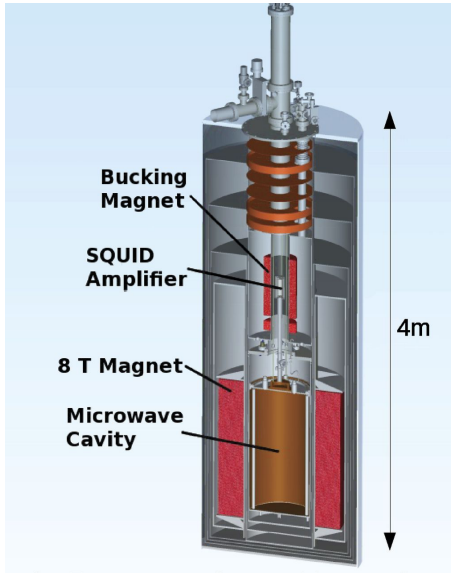


Figure 18: The schematic of the ADMX experiment [76]. The cavity of diameter 0.5 m and length 1.0 m, is inside the bore of an 8.5 T Niobium-Titanium (NbTi) superconducting magnet.

The ADMX experiment has currently searched in the range  $1.9 \times 10^{-6}$  eV  $\leq m_A \leq 3.65 \times 10^{-6}$  eV, or between 460 and 890 MHz [77, 78]. These results are shown Figure 8 (and later in Figures 24 - 26). It excluded, at a 90% CL, the possibility of KSVZ axions in the mass range  $1.9 \times 10^{-6}$  eV  $< m_A < 3.53 \times 10^{-6}$  eV [79]. However, they were then revived in this limit due to the uncertainty value of  $z = m_u/m_d = 0.56$ , which can actually hold a value between 0.35 and 0.60 [80].

A second ADMX platform, the ADMX-HF, was constructed with the intention of researching and developing technologies and techniques in the search for axions and ALPs. This is discussed further in Section 7.3.

### 6.4.2 Bragg diffraction scattering

Axions can convert into X-ray photons coherently when the incident angle of an axion with a crystal plane satisfies the Bragg condition [21, 81, 82]. This is due to the crystal's atomic electric field. When the Bragg condition is satisfied the signal is enhanced by up to a factor of  $10^4$  into the observable range [82]. The experiments COSME and SOLAX used germanium (Ge) detectors to find coupling limits of  $g_{A\gamma\gamma} \lesssim 2.7 \times 10^{-9} \text{ GeV}^{-1}$  [83, 84], another (DAMA) used NaI to attain a limit of  $g_{A\gamma\gamma} \lesssim 1.7 \times 10^{-9} \text{ GeV}^{-1}$  [85]. Figure 19 displays these results.

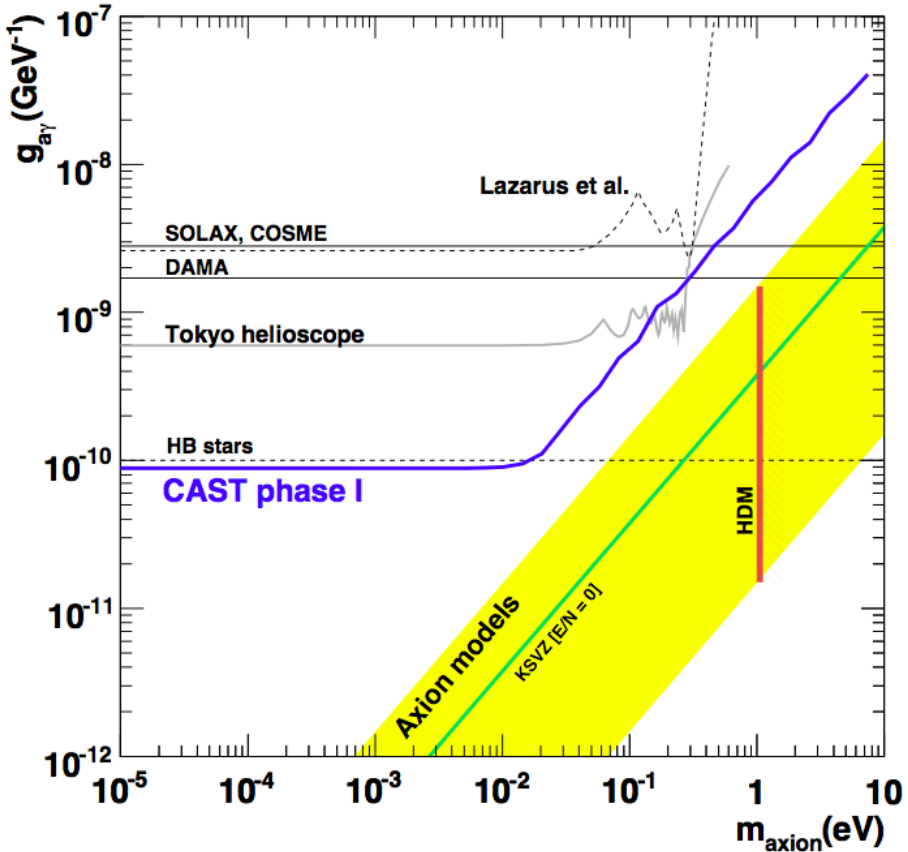


Figure 19: A graph of  $g_{a\gamma} (\text{GeV}^{-1})$  vs.  $m_A$  (eV) displaying the exclusion limits from COSME, SOLAX, and DAMA in comparison to the axion model band, limits from HB stars and hot dark matter (HDM) and other experimental constraints [27].

This experimental technique, however, does not compete with helioscope abilities to reach much higher sensitivities. To combat this, these detectors could be used to detect solar axions through the axio-electric effect. An incoming axion of energy causes an electron to recoil with equal energy [21]. The sensitivity of this would still not be enough to detect QCD axions.

#### 6.4.3 Searches in dark matter direct detection experiments

The EDELWEISS-II experiment searches for axions with a target mass of Ge through the detection of electron recoils. Whether the axion couples to photons or electrons determines what process to search for. For example, in EDELWEISS-II, the inverse Primakoff effect and the axio-electric effect were searched for via electron recoil in Ge bolometers.

The EDELWEISS collaboration set a 95% CL limit on the coupling to photons  $g_{A\gamma} < 2.13 \times 10^{-9} \text{ GeV}^{-1}$  in a mass range not fully probed by axion helioscopes. They also constrained the axion-electron coupling  $g_{Ae} < 2.56 \times 10^{-11} \text{ GeV}^{-1}$  for  $m_A < 10^{-3} \text{ eV}$ , and limited  $g_{Ae} \times g_{eff}^{AN} < 4.70 \times 10^{-17} \text{ GeV}^{-1}$  where  $g_{eff}$  is the effective axion-nucleon coupling for  $^{57}\text{Fe}$ . Figure 20 displays the axion-electron constraints. These results mean that EDELWEISS-II can fully exclude the mass range  $0.91 \text{ eV} < m_A < 80 \times 10^{-3} \text{ eV}$  for DFSZ axions and  $5.73 \text{ eV} < m_A < 40 \times 10^{-3} \text{ eV}$  for KSVZ axions [21].

Another experiment XENON100, exploits the axio-electric effect in the same way as EDELWEISS-II, but with a different target mass of liquid xenon (LXe). No signal was found, but through null observation the following constraints were imposed [86]. The solar axion coupling was excluded at a 90% CL for  $g_{Ae} > 7.7 \times 10^{-12}$ . QCD axions were excluded in the regions  $m_A > 0.3 \text{ eV}$  for DFSZ axions, and  $m_A > 80 \text{ eV}$  for KSVZ axions. For ALPs, assuming that they constitute the entire dark matter population of our galaxy,  $g_{Ae} < \times 10^{-12}$  at a 90% CL for masses between 5 and 10 keV. Figure 21b displays these results.

In addition to these limits, the XMASS project produced another set of constraints, using LXe as the target [87]. XMASS again detects axions through the axio-electric effect, but this time searches for solar axions that have been produced through Compton-like scattering and the bremsstrahlung process. XMASS constrained a model-independent limit on the coupling for masses  $\ll 1 \times 10^3 \text{ eV}$  as  $g_{aee} < 5.4 \times 10^{-11}$  at a 90% CL. Figure 20 displays the constraints found for the axion-electron coupling. Red giants show the strongest constraint, as mentioned in Section 5.1 . The bounds on the axion masses for the DFSZ and KSVZ axion models were 1.9 and 250 eV respectively. In the mass range  $1 \times 10^4 \leq m_A \leq 4 \times 10^4 \text{ eV}$ , this study improved the limits that were previously derived from astrophysical observations [88].

## 7 Prospects for axion and ALP searches in the near future

This section considers the future of the methods of detection previously discussed in Section 6. The current and projected improvements being made to these experiments are discussed. Then current experiments that could have the sensitivity to detect axions are examined. Furthermore, new proposed experimental methods are reviewed.

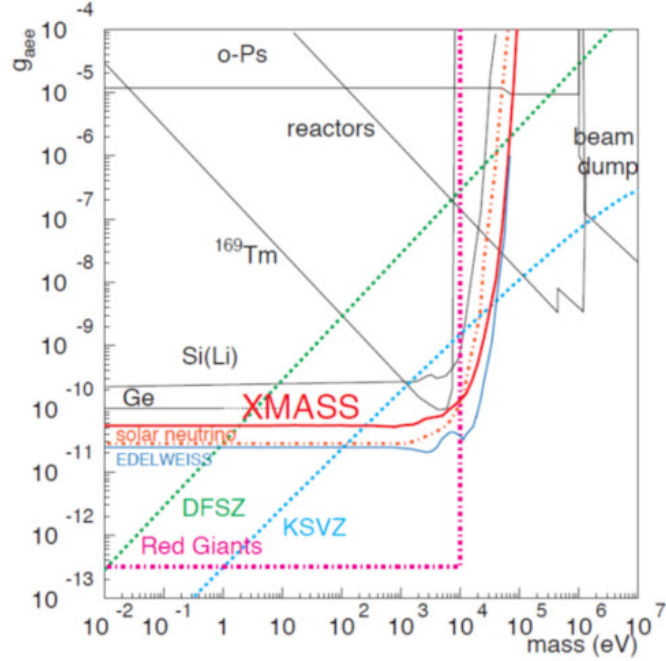
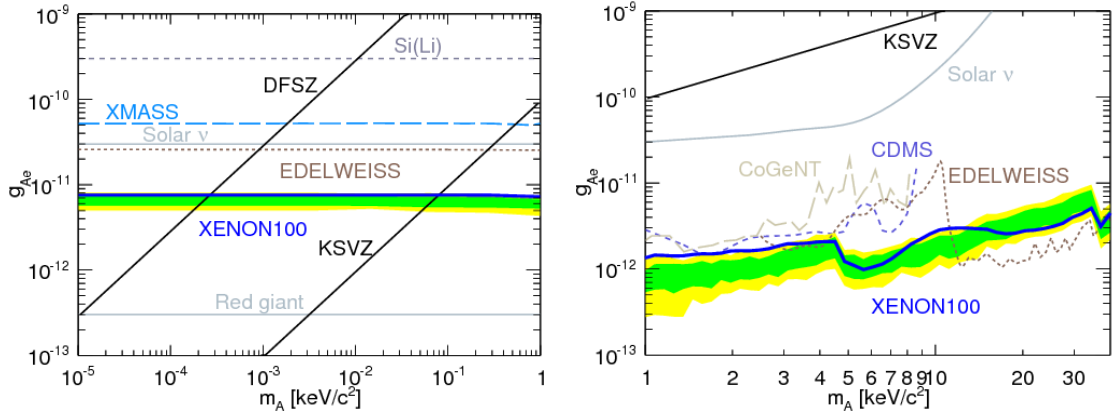


Figure 20: A graph of  $g_{aee}$  ( $\text{GeV}^{-1}$ ) vs.  $m_A$  (eV) for XMASS results with a 90% CL [87].



(a) The limits on solar axions, indicated by the blue line with (90% CL).

(b) The limits on ALPs, indicated by the blue line with 90% CL.

Figure 21: Graphs of  $g_{Ae}$  ( $\text{GeV}^{-1}$ ) vs.  $m_A$  ( $\text{keV}/c^2$ ) for solar axions (a) and ALPs (b), from the XMASS experiment [86]. Indirect astrophysical bounds from solar neutrinos and red giants are represented by dashed lines. The expected sensitivity is shown by the green and yellow bands. The benchmark DFSZ and KSVZ models are represented by grey dashed lines. The ALP limits are made under the assumption that ALPs constitute all of the dark matter in our galaxy.

## 7.1 Photon regeneration experiment improvements

The next generation of the ALPS experiment, ALPS-IIc, is currently improving sensitivity by: increasing the magnet length, to increase the size of the photon regeneration space; introducing a regeneration cavity, to boost the probability of regeneration; and adding an improved detector system, to improve single-photon detection. The main sensitivity gain is due to the enhanced magnet length arising from the use of two ‘HERA-dipole’ magnets, rather than just one. ALPS-II expects a sensitivity improvement of  $3 \times 10^3$  [57]. Figure 22 displays the prospected sensitivities.

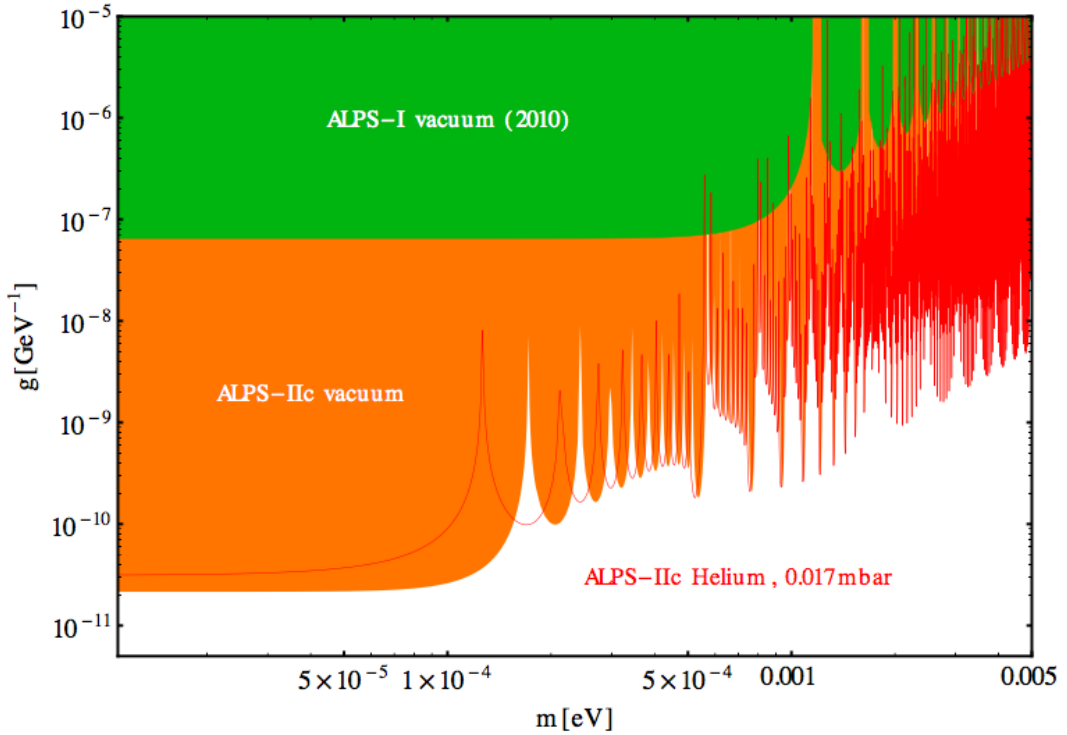


Figure 22: A graph of  $g_- (\text{GeV}^{-1})$  vs.  $m_A$  (eV) showing the prospective sensitivity for ALPs in the final stage of the ALPS experiment, ALPS-IIc (orange), compared to previous reported sensitivities for ALPS (green). [89].

## 7.2 Helioscope improvements

The next generation of axion helioscope has already been conceptualised and designed, although there is little motivation to go to yet larger masses in a helioscope search due to the cosmic hot dark matter bound of  $m_A < 0.7$  eV [90]. The International Axion Observatory (IAXO) [91] will be a fourth generation helioscope, with the main task of searching for axions or ALPs. The apparatus will consist of a 20m-long 8-coils toroidal superconducting magnet within a cryostat. The magnet bores will be equipped with X-ray optics which will focus the signal photons on ultra-low-background ‘Micromegas’ X-ray detectors [92]. Figure 24 displays a diagram of the

IAXO helioscope. IAXO will be about  $10^{4-5}$  times more sensitive than CAST, with the ability to search for axion-photon couplings down to the  $g_{A\gamma\gamma} \lesssim 10^{-12} \text{ GeV}^{-1}$  limit. This will push the sensitivity of the product of couplings  $g_{A\gamma\gamma}g_{Aee}$ , beyond the stellar energy-loss limits and have the ability to test whether axion emission dominates WD cooling. Figure 24 shows the projected sensitivities for IAXO in comparison to CAST.

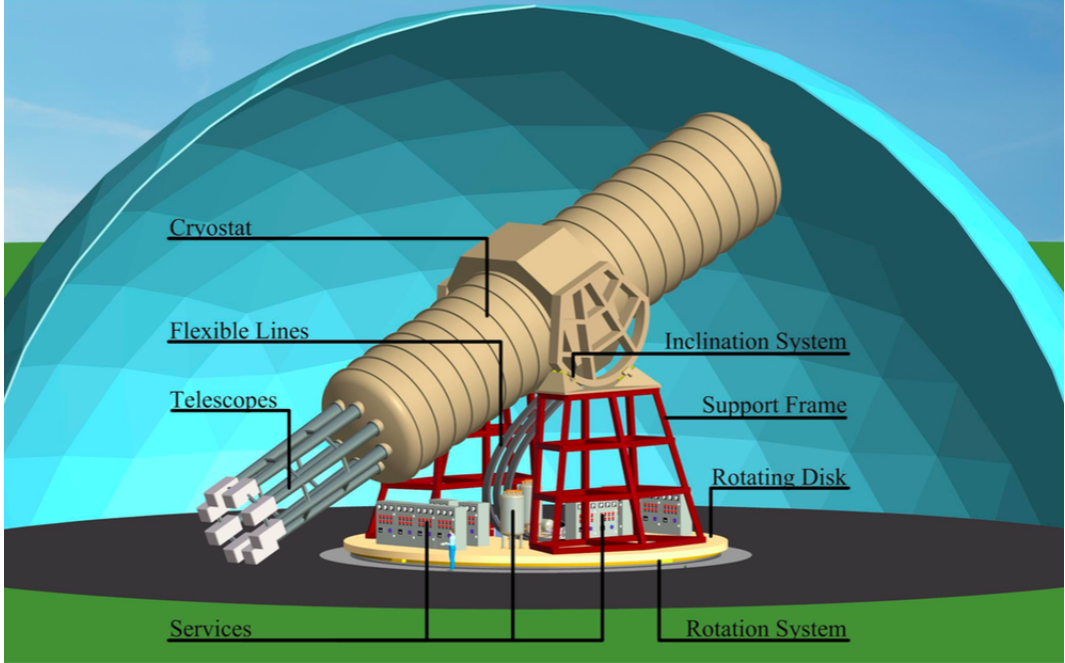


Figure 23: A diagram of the proposed IAXO helioscope [92].

### 7.3 Haloscope improvements

The next generation of the haloscope aims at scanning the entire mass range, from  $1 \times 10^{-6} \leq m_A \leq 1 \times 10^{-3} \text{ eV}$ . However, this requires quite significant technological advances to maintain current sensitivity at higher frequencies.

The cavity and amplifier technology is the focus of the research and development of haloscope experiments, as these are what improve sensitivity and speed. One particular avenue of development is the reduction of temperature of the SQUID amplifiers of the ADMX experiment. A dilution refrigerator is currently being incorporated into the apparatus, and will enable it to achieve a noise temperature of less than 200 mK. This would increase sensitivity to dark matter axion couplings between  $1 \times 10^{-6} \text{ eV}$  and  $10 \times 10^{-6} \text{ eV}$ . Figure 25 displays the projected sensitivities of the ADMX experiment once the dilution refrigerator is installed [93].

The ADMX-HF experiment uses a NbTi magnet just as ADMX (Section 6.4), but has a higher magnetic field strength of 9.4 T. It was specifically designed to have a high field uniformity

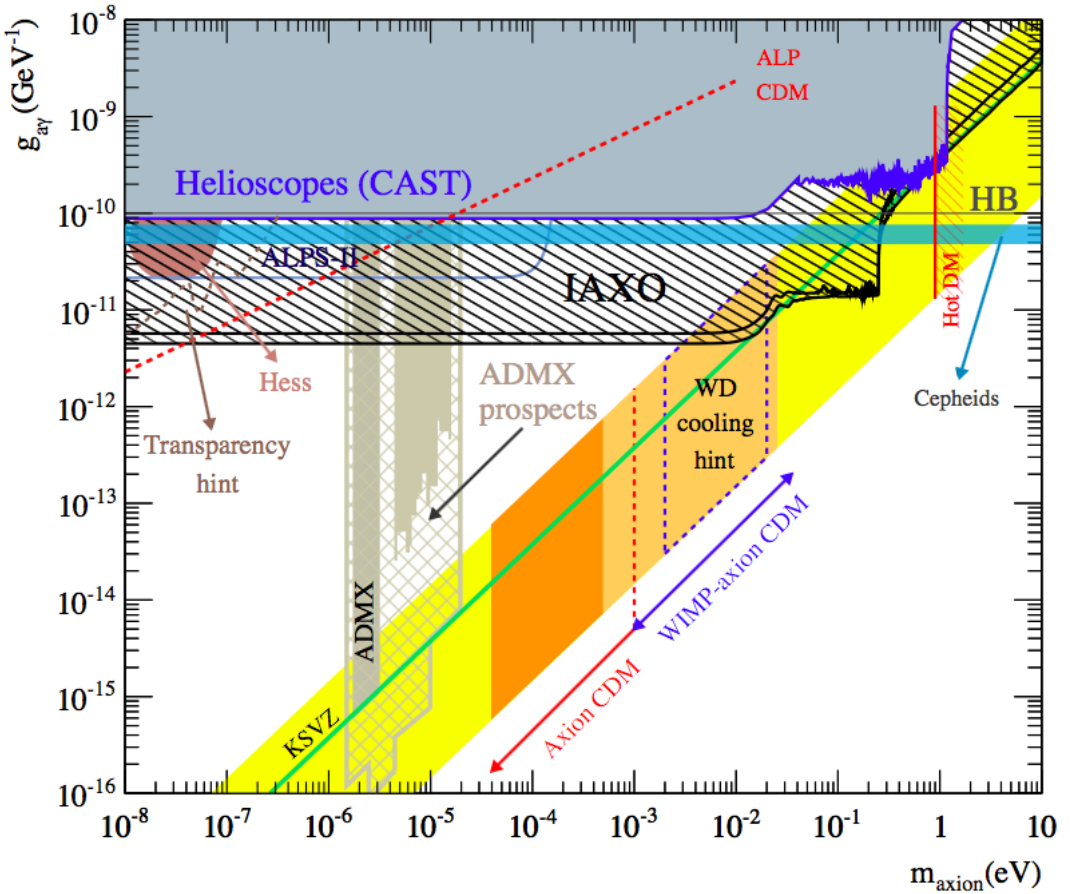


Figure 24: A graph of  $g_{A\gamma}$  ( $\text{GeV}^{-1}$ ) vs.  $m_A$  (eV) of the IAXO sensitivity in comparison to previous experimental, astrophysical and cosmological constraints, and axion models. [94].

to allow for testing thin-film superconducting cavities. This experiment incorporated a dilution refrigerator from the outset and is projected to reach an unprecedented sensitivity in axion-photon coupling. The focus of the development and research of the ADMX-HF is on boosting the axion-photon conversion power and the speed of the scanning, and trying to evade the quantum limit in noise. The conversion power, and therefore speed, will be improved through incorporating Type-II superconducting thin films on all of the cylindrical surfaces of the microwave cavity to boost the quality factor by an order of magnitude. The quantum noise limit evasion will be attempted through a receiver based on squeezed-vacuum states, previously employed in apparatus such as LIGO and GEO [95, 96]. The system noise could possibly be reduced to a tenth of the quantum limit through reducing naturally occurring vacuum fluctuations with a squeezed vacuum. With all of these developments, this experiment could ultimately reach DFSZ sensitivity. ADMX-HF has recently published its first set of results, excluding axion models coupling a factor of 2.3 above the benchmark KSVZ model,  $g_{A\gamma\gamma} \gtrsim 2 \times 10^{-14} \text{ GeV}^{-1}$ , over the mass range  $2.355 \times 10^{-5} \text{ eV} < m_A < 2.40 \times 10^{-5} \text{ eV}$ . These are the first limits within

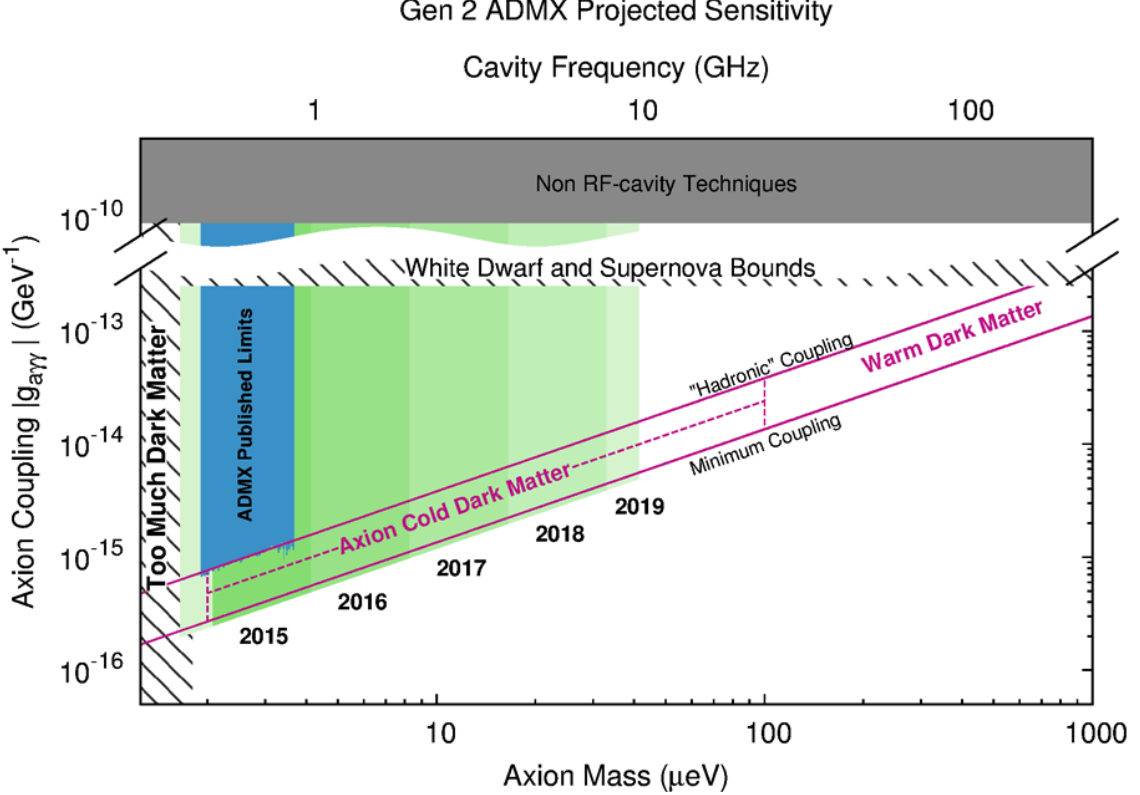


Figure 25: A graph of  $g_{A\gamma\gamma}$  ( $\text{GeV}^{-1}$ ) vs.  $m_A$  ( $\mu\text{eV}$ ) the projected sensitivity of the next stage of ADMX [93]. The sensitivity the ADMX-HF apparatus is also displayed.

the axion model band in the mass decade above  $1 \times 10^{-5}$  eV. Figure 26 displays these results in comparison to the model bands.

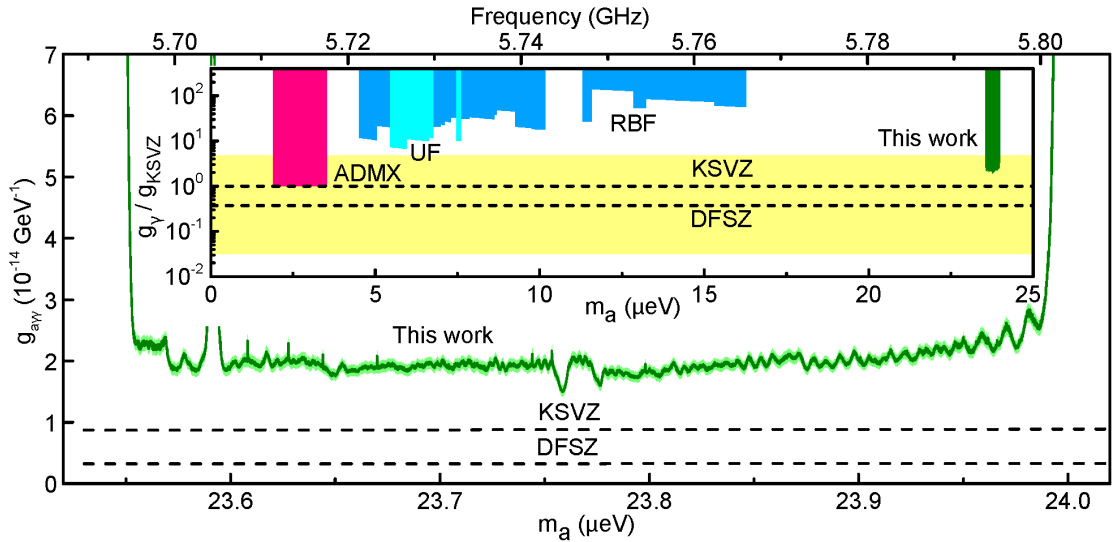


Figure 26: A graph of  $g_{A\gamma\gamma}$  ( $\times 10^{-14}$  ( $\text{GeV}^{-1}$ )) vs.  $m_A$  ( $\mu\text{eV}$ ) showing the first results from the ADMX-HF experiment (green) [97].

## 7.4 Detection using atomic transitions

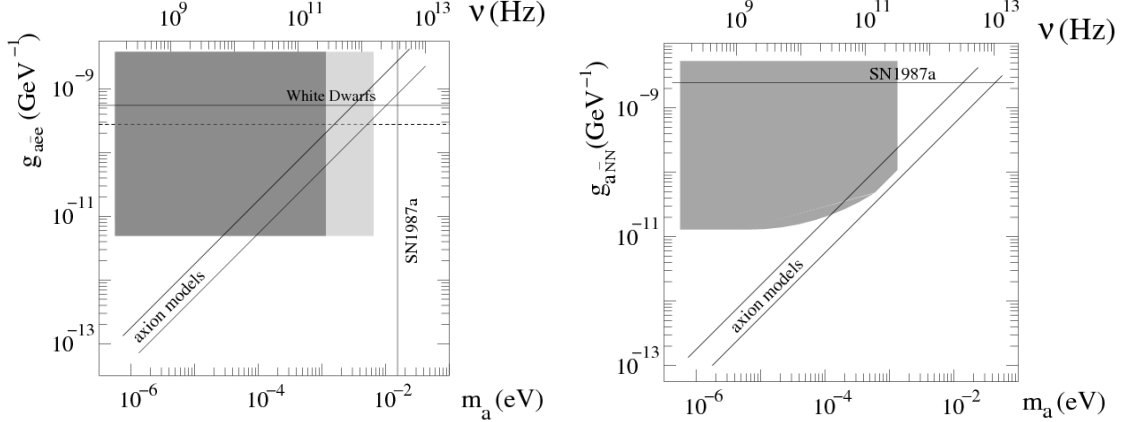
A recently proposed axion detection method is through atomic transitions in which axions can be absorbed. For most atoms, each ground state can be accompanied by other states that have had the spin of one or more valence electrons flipped, or have had the z-component of the nuclear spin changed. The Zeeman effect could be used to tune the difference in energy between these states [35]. The transitions could then be detected using a laser that has its frequency set to cause transitions from one state to an excited state with energy of the order of an eV above the ground state, but would not cause transitions from low energy states. Thus, when the atom de-excites, a photon is emitted and counted. Dark matter axions may cause these transitions, which would cause the emission of a photon of an energy equal to that of the axion mass. P. Sikivie (2014) proposes to search for this effect through the cooling of a kilogram-sized sample to mK temperatures, then counting the axion induced transitions using laser techniques. This method would allow detection of axions in the  $10^{-4}$  eV mass range. The possible search ranges from axion-electron coupling and axion-nucleon coupling are displayed in Figures 27a and 27b, with the former showing the possible search range extension in the lighter shaded area if suitable target materials are found. The search would be done through the use of paramagnetic materials, however could be improved to higher frequencies through the use of anti-ferromagnetic materials.

## 7.5 Detection using nuclear magnetic resonance (NMR)

The Cosmic Axion Spin Precession Experiment (CASPER) [98] has begun construction and, upon completion, aims to explore the range  $10^{-6} \leq m_A \leq 10^{-9}$  eV by detecting spin precession caused by axions through the use of NMR [99].

This proposed range covers low frequencies from energies  $f_A \sim 10^{15} - 10^{19}$  GeV, which is challenging for most techniques outside of the astrophysical constraining methods. This experiment will be able detect any light particle that couples to nucleons, so it could be very interesting to the wider dark matter search, but it is particularly interesting for axion detection due to this projected (and currently unattained) frequency range.

The CASPER detection methods split into searches for two different couplings, as discussed in Reference [98]: CASPER-Wind would search for the axion-nucleon coupling, where the nuclear spins precess around the local velocity of the dark matter; and CASPER-Electric would search for the nucleon electric dipole moment (EDM) that has been induced by the axion [99]. Here the nuclear EDM causes the magnetic moment to precess around an effective electric field in the crystal [98]. The frequency at which they do this is called the Larmor frequency. Using the fact that the wind and the EDM vary with time, there would be a precession of a nucleon spin around the spatial gradient of the local axion dark matter field in a sample of matter. CASPER



(a) A graph of  $g_{Aee}$  ( $\text{GeV}^{-1}$ ) vs.  $m_A$  (eV) displaying the expected sensitivity of the coupling of the axion to electrons using atomic transitions as the detection method.

(b) A graph of  $g_{ANN}$  ( $\text{GeV}^{-1}$ ) vs.  $m_A$  (eV) displaying the expected sensitivity of the coupling of the axion to nuclei.

Figure 27: The diagonal lines are the predictions of models with  $g_e, g_N = 1.0$  and 0.3 [35]. Figure a) The horizontal dotted line is the coupling that yields a best fit to the white dwarf cooling observations. The shaded area indicates the projected sensitivity of the proposed detector, using electron paramagnetic resonance (dark) and anti-ferromagnetic resonance (light). Figure b) The shaded area indicates the expected sensitivity of the proposed detector.

could possibly be used to search for the spin of axio-electric coupling but that would not be sensitive enough to advance the current axion parameter space limits [99].

The Larmor frequency of the spins would be scanned through ‘ramping’ of the magnetic field until the frequency that corresponds to the mass of an axion is met. This transverse magnetisation could be measured with a SQUID, as shown in Figure 28. As CASPER-Wind would not require an applied electric field liquid xenon (LXe) can be used as the matter sample as NMR techniques have already been demonstrated in this target medium. Technologies have not yet been demonstrated for the other search strategies. CASPER-Electric would require more complex ferroelectric materials or polar crystals with large internal electric fields in order to achieve the projected sensitivity [99].

## 7.6 Direct detection experiments

Direct detection searches with 10 – 100 times higher target mass than the results discussed in Section 6 are currently operating (Edelweiss-III, DEAP-3600, Xenon-1T) or planned for the near future (DarkSide-20k, LZ). The sensitivity of such experiments to the axio-electric effect

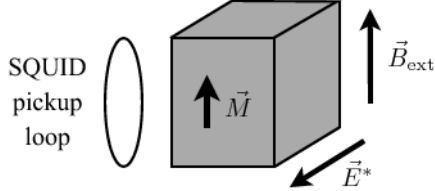


Figure 28: A diagram of the geometry of the NMR experiment [98]. The applied magnetic field  $\vec{B}_{ext}$  is colinear with the sample magnetisation,  $\vec{M}$ . The effective electric field in the crystal  $\vec{E}$  is perpendicular to  $\vec{B}_{ext}$ .

scales with the target mass, assuming that the same level of background discrimination against electron and gamma backgrounds can be maintained.

For example the Dark Matter Experiment using Argon Pulse-shape discrimination (DEAP-3600) achieves high sensitivity through: reduction in the radioactivity of the components, the use of argon which has a large target mass, and the reduction in background radiation by locating the detector in the SNOLAB facility which is 2km underground [100]. This detector searches for dark matter particle interactions in a 1000 kg fiducial target mass of liquid argon. The target sensitivity is  $10^{-46} \text{ cm}^2$  of the scattering of Weakly Interacting Massive Particles (WIMPs) on nucleons [100]. Sensitivity over current searches will increase by an order of magnitude at a 100GeV WIMP mass. The sensitivity of the apparatus can be extended to the axion search. DEAP-3600 aims to produce results in the near future. In addition to this, the next stage of DEAP has been proposed and is being developed with a 50-tonne fiducial argon target mass. This could improve sensitivity by another factor of 100.

## 8 Conclusions

This review investigates the axion and ALPs with respect to their properties, their production mechanisms, their ability to contribute to the dark matter population of the universe, and their detection.

Axions are the consequence of a theorised solution to the strong CP problem. There are two leading models of the axion: the DFSZ model, which is a GUT and can couple to SM quarks and leptons; and the KSVZ model, which is a hadronic model and only couple to SM heavy quarks. The mass of the axion, and the coupling of axions to photons, electrons and nucleons, are related through the energy scale parameter  $f_A$ . The mechanisms which employ these couplings are Primakoff production, Compton-like scattering, bremsstrahlung, axio-recombination, axio-deexcitation and the nuclear magnetic transition of  $^{57}\text{Fe}$  nuclei. Which mechanism dominates the axion production and, therefore, axion flux, depends on the environment and the model

considered (except for the nuclear magnetic transition of  $^{57}\text{Fe}$  nuclei which does not have a strong model dependence).

ALPs differ in the fact that mass is disproportionate to coupling. They are pseudoscalar particles that have a much larger parameter search space than axions and they do not necessarily solve the CP problem. The motivation of ALPs instead comes from string theory. As a result, the restraints on the ALP parameter space are less stringent.

QCD axions are natural candidates for cold dark matter. The various cold dark matter production mechanisms – vacuum realignment, string decay, and domain wall decay – imply constraints of  $f_A \lesssim 10^{12} \text{ GeV } \theta_i^{-2}$ , for  $m_A \geq 10^{-6} \text{ eV } \theta_i^{-2}$  [?]. Axions have also been postulated as a BEC, which motivates their compatibility as a dark matter particle.

The proposal of the existence of axions and ALPs is interesting for extensions to SM theories, and for dark matter particle candidacy. As a result there is a very active experimental search programme in operation. Astrophysical constraints from solar axions causing stellar energy loss have been examined, as have the conversion of photons to axions (and back again) in large scale magnetic fields, such as the Earth's magnetosphere. Laboratory searches are attempting to directly detect axions through: photon regeneration, birefringence and dichroism, helioscopes, and haloscopes. With each experiment and increase in sensitivity, the searches constrain the axion and ALP parameter space more.

This review has shown that the axion has a well bounded parameter space for mass  $m_A$ , various couplings and  $f_A$ . From constraints imposed by cosmology, astrophysics and experimental non-observation of axions and ALPs, the generally accepted ‘axion window’ exists in the range  $1 \times 10^{-6} \leq m_A \leq 1 \times 10^{-3} \text{ eV}$ , or  $4 \times 10^8 \text{ GeV} < f_A < 10^{12} \text{ GeV}$ . Dark matter QCD axions are constrained even further to  $1 \times 10^{-6} \leq m_A \leq 1 \times 10^{-4} \text{ eV}$ . The ALP parameter space is much larger in comparison, with ambiguous, conflicting limits on its size from various sources. Figure 29 represents the current constraints of the axion- and ALP-photon coupling  $g_{A\gamma}$  obtained from the numerous measurements considered in this review.

The next steps in the axion and ALP search promise even higher sensitivities in each of the detection methods. As technology improves and the parameter space is bound more, the possible detection of the axion or ALP gets closer. The development of new search techniques such as detection using atomic transitions or NMR could search and constrain or detect axions or ALPs new parameter spaces. The most promising approaches to the detection of the QCD dark matter axion are through the microwave cavity haloscope and direct detection experiments. The next generation of haloscope, IAXO, and experiments such as DEAP-3600 would explore the parameter space with an unprecedented sensitivity.

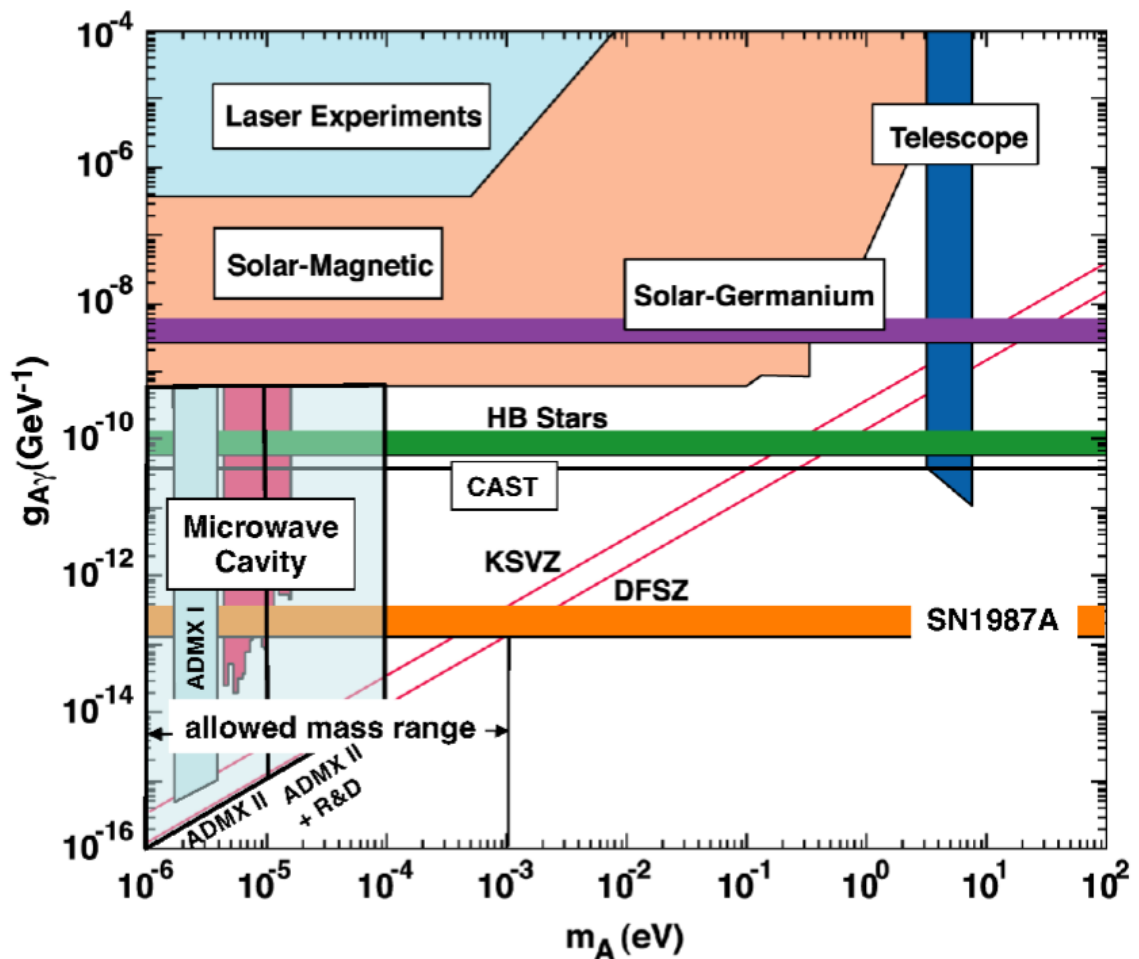


Figure 29: A graph of  $g_{A\gamma}$  ( $\text{GeV}^{-1}$ ) vs.  $m_A$  ( $\text{GeV}$ ) of the current constrained ALP parameter space [1].

## References

- [1] A. Kusenko, L. J. Rosenburg *Snowmass-2013 Cosmic Frontier 3 (CF3) Working Group Summary: Non-WIMP dark matter.* (2013); ePrint arXiv:1310.8642.
- [2] H.Y. Cheng. The Strong CP Problem Revisited. *Phys. Rept.* **158** (1988) 1; DOI: 10.1016/0370-1573(88)90135-4.
- [3] H. Greaves, T. Thomas. The CPT Theorem. *Studies in History and Philosophy of Modern Physics* **45** (2014) pp. 46-66; ePrint arXiv:1204.4674v1.
- [4] J.R. Fry. CP violation and the standard model *Reports on Progress in Physics.* **63** 2 (2000) pp. 117-169; DOI: 10.1088/0034-4885/63/2/202.
- [5] H. Banerjee, D. Chatterjee and P. Mitra. Is there still a strong CP problem? *Phys.Lett.* **B573** 109 (2003); ePrint arXiv:hep-ph/0012284.
- [6] F. Wilczek. QCD Made Simple. *Phys. Today* **53**, 8 (2000) 22; DOI: 10.1063/1.1310117.
- [7] R.L Oldershaw. The Meaning Of The Fine Structure Constant. (2009); ePrint arXiv:0708.3501v2.
- [8] E.V. Shuryak. The QCD Vacuum, Hadrons and Superdense Matter. World Scientific Publishing Co., Hackensack, 2004, pp. 77-78.
- [9] Laure Gouba. The Yukawa Model in One Space-One time Dimensions. (2016); ePrint arXiv:1608.03504.
- [10] C. A. Baker, D. D. Doyle, P. Geltenbort, K. Green, M. G. D. van der Grinten, *et al.* *Phys. Rev. Lett.* **97** 131801 (2006); ePrint arXiv:hep-ex/0602020v3.
- [11] R.D. Peccei, H. R. Quinn. CP Conservation in the Presence of Pseudoparticles. *Phys. Rev. Lett.* **38**(25) (1977) pp. 1140-1143; DOI: 10.1103/PhysRevLett.38.1440.
- [12] R.D. Peccei, H. R. Quinn. Constraints Imposed by CP Conservation in the Presence of Pseudoparticles. *Phys. Rev.* **D16**(6) (1977) pp. 1791-1797; DOI: 10.1103/PhysRevD.16.1791.
- [13] F. Wilczek. Problem of Strong P and T Invariance in the Presence of Instantons. *Phys. Rev. Lett.* **40**279 (1978) 279-282; DOI: 10.1103/PhysRevLett.40.279.

- [14] Y. Nambu. Quasi-Particles and Gauge Invariance in the Theory of Superconductivity. *Phys. Rev.* **117** (1960) 648; DOI: [10.1103/PhysRev.117.648](https://doi.org/10.1103/PhysRev.117.648).
- [15] J. Goldstone. Field Theories with Superconductor Solutions. *Nuovo Cim.* **19** (1961) 154-164; DOI: [10.1007/BF02812722](https://doi.org/10.1007/BF02812722).
- [16] S. Weinberg. A New Light Boson? *Phys. Rev. Lett.* **40** 223 (1978); DOI: [10.1103/PhysRevLett.40.223](https://doi.org/10.1103/PhysRevLett.40.223).
- [17] J.E. Kim, G. Carosi. Axions and the Strong CP Problem. *Rev. Mod. Phys.*, **82** (2010) pp. 557-602; DOI: [10.1103/RevModPhys.82.557](https://doi.org/10.1103/RevModPhys.82.557).
- [18] J. Preskill, M.B. Wise, F. Wilczek. Cosmology of the Invisible Axion. *Phys. Lett.* **B120** 127 (1983). DOI:[10.1016/0370-2693\(83\)90637-8](https://doi.org/10.1016/0370-2693(83)90637-8)
- [19] L.F. Abbott, P. Sikivie. A cosmological bound on the invisible axion. *Phys. Lett.* **B120** 133; DOI: [10.1016/0370-2693\(83\)90638-X](https://doi.org/10.1016/0370-2693(83)90638-X).
- [20] M. Dine and W. Fischler. The Not So Harmless Axion. *Phys. Lett.* **B120** (1983) 137; DOI: [10.1016/0370-2693\(83\)90639-1](https://doi.org/10.1016/0370-2693(83)90639-1).
- [21] The EDELWEISS Collaboration: E. Armengaud *et al.* Axion searches with the EDELWEISS-II experiment. *JCAP* **1311** (2013); ePrint [arXiv:1307.1488v1](https://arxiv.org/abs/1307.1488v1).
- [22] J. Redondo. Axions at the International Axion Observatory. (2015) ePrint arXiv: [1601.00578v1](https://arxiv.org/abs/1601.00578v1).
- [23] CAST Collaboration (Andriamonje, S. *et al.*) Search for 14.4-keV solar axions emitted in the M1-transition of Fe-57 nuclei with CAST. *JCAP* **0912** (2009) 002; ePrint arXiv:0906.4488.
- [24] M. Srednicki. Axion couplings to matter: (I). CP-conserving parts. *Nucl.Phys. B* **2603-4** (1985) pp. 689-700; DOI: [10.1016/0550-3213\(85\)90054-9](https://doi.org/10.1016/0550-3213(85)90054-9).
- [25] K.A. Olive *et al.* (Particle Data Group) *Chinese Physics*, **C38** 090001 (2014) 626-633; DOI: [10.1088/1674-1137/38/9/090001](https://doi.org/10.1088/1674-1137/38/9/090001).
- [26] G.G. Raffelt. Astrophysical Methods to Constrain Axions and Other Novel Particle Phenomena. *Phys. Rep.* **198**(1-2) (1990) pp. 1-113; DOI: [10.1016/0370-1573\(90\)90054-6](https://doi.org/10.1016/0370-1573(90)90054-6).

- [27] The CAST Collaboration. An improved limit on the axion-photon coupling from the CAST experiment. *JCAP* **2007**04 (2007) pp. 10; DOI: 10.1088/1475-7516/2007/04/010.
- [28] The Fermi-LAT Collaboration: M. Ajello *et al.* Search for Spectral Irregularities due to Photon-Axion-like-Particle Oscillations with the Fermi Large Area Telescope. *Phys. Rev. Lett.* **116** (2016) 161101; ePrint arXiv:1603.06978v2.
- [29] P. Svrcek, E. Witten. Axions in String Theory. *JHEP* **0606** (2006) 051; ePrint arXiv:hep-th/0605206v2.
- [30] G. Raffelt. Warsaw Workshop on Non-Standard Dark Matter. (2016) Available Online: <http://indico.fuw.edu.pl/getFile.py/access?contribId=24&sessionId=9&resId=1&materialId=slides&confId=45>. Accessed: 4 Nov 2016.
- [31] J.L. Feng *et al.* Planning the Future of U.S. Particle Physics (Snowmass 2013): Chapter 4: Cosmic Frontier. *FERMILAB-CONF-14-019-CH04*. (2014); e-Print arXiv:1401.6085.
- [32] L.D. Duffy, K. van Bibber. Axions as Dark Matter Particles. *New J. Phys.* **11**:105008 (2009); ePrint arXiv:0904.3346v1.
- [33] E. Massó, R. Toldrà. New constraints on a light spinless particle coupled to photons. *Phys. Rev.* **D55** 7967 (1997); DOI: 10.1103/PhysRevD.55.7967.
- [34] P. Sikivie. Axion Cosmology *Lect. Notes Phys.* **741**, 19 (2008); ePrint arXiv:astro-ph/0610440.
- [35] P. Sikivie. Axion Dark Matter Detection using Atomic Transitions. *Phys. Rev. Lett.* **113** (2014) 20, 201301; DOI: 10.1103/PhysRevLett.113.201301
- [36] P. Sikivie, Q. Yang. Bose-Einstein Condensation of Dark Matter Axions. *Phys. Rev. Lett.* **103**, 111301 (2009) DOI: 10.1103/PhysRevLett.103.111301.
- [37] N. Banik and P. Sikivie. Axions and the galactic angular momentum distribution. *Phys. Rev. D* 88, 123517; DOI: 10.1103/PhysRevD.88.123517
- [38] L.D. Duffy, P. Sikivie. The Caustic Ring Model of the Milky Way Halo. *Phys. Rev.* **D78** (2008) 063508 DOI: 10.1103/PhysRevD.78.063508.
- [39] P. Sikivie. The emerging case for axion dark matter. *Phys. Lett.* **B695** (2011) pp. 22-25 DOI: 10.1016/j.physletb.2010.11.027.

- [40] J. Redondo. Solar axion flux from the axion-electron coupling. (2013); ePrint [arXiv:1310.0823v1](https://arxiv.org/abs/1310.0823v1).
- [41] F. Alessandria *et al.*, Search for 14.4 keV solar axions from M1 transition of Fe-57 with CUORE crystals, *JCAP* **05** (2013) 007; DOI: [10.1088/1475-7516/2013/05/007](https://doi.org/10.1088/1475-7516/2013/05/007)
- [42] H. Schlattl, A. Weiss, G. Raffelt. Helioseismological constraint on solar axion emission. *Astropart. Phys.* **10** (1999) pp. 353–359; DOI: [10.1016/S0927-6505\(98\)00063-2](https://doi.org/10.1016/S0927-6505(98)00063-2).
- [43] P. Gondolo, G. Raffelt. Solar neutrino limit on axions and keV-mass bosons. *Phys. Rev.* **D79** (2009) 107301; DOI: [10.1103/PhysRevD.79.107301](https://doi.org/10.1103/PhysRevD.79.107301).
- [44] G. G. Raffelt. Particle physics from stars. *Ann. Rev. Nucl. Part. Sci.* **49** (1999) 163–216; DOI: [10.1146/annurev.nucl.49.1.163](https://doi.org/10.1146/annurev.nucl.49.1.163).
- [45] G.G. Raffelt. Axion constraints from white dwarf cooling times. *Phys. Let. B* **166** 4 (1986) pp. 402-406; DOI: [10.1016/0370-2693\(86\)91588-1](https://doi.org/10.1016/0370-2693(86)91588-1).
- [46] J. Isern, E. Garcia-Berro, S. Torres, S. Catalan. Axions and the cooling of white dwarf stars. *Astrophys. J. L.* **682** (2008); DOI: [10.1086/591042](https://doi.org/10.1086/591042).
- [47] G. Raffelt, A. Weiss. Red giant bound on the axion - electron coupling revisited. *Phys.Rev. D51* (1995) pp. 1495-1498; DOI: [10.1103/PhysRevD.51.1495](https://doi.org/10.1103/PhysRevD.51.1495).
- [48] D.B. Kaplan. Opening the Axion Window. *Nucl. Phys.* **B260** (1985) 215-226; DOI: [10.1016/0550-3213\(85\)90319-0](https://doi.org/10.1016/0550-3213(85)90319-0).
- [49] H.S. Hudson. X-Ray Searches for Solar Axions. (2012) ePrint arXiv: [1201.4607](https://arxiv.org/abs/1201.4607).
- [50] G.W. Fraser, A.M. Read, S. Sembay, J.A. Carter, E. Schyns. Potential solar axion signatures in X-ray observations with the XMM–Newton observatory. *Mon. Not. Roy. Astron. Soc.* **445** 2 (2014) pp. 2146-2168; DOI: [10.1093/mnras/stu1865](https://doi.org/10.1093/mnras/stu1865).
- [51] J.W. Brockway, E.D. Carlson, and G.G. Raffelt. SN 1987A Gamma-Ray Limits on the Conversion of Pseudoscalars. *Phys. Lett. B* **383** 439 (1996); DOI: [10.1016/0370-2693\(96\)00778-2](https://doi.org/10.1016/0370-2693(96)00778-2).
- [52] J. Engel, D. Seckel, A. Hayes. Emission and detectability of hadronic axions from SN1987A. *Phys. Rev. Lett.* **65** (1990) 960–963; DOI: [10.1103/PhysRevLett.65.960](https://doi.org/10.1103/PhysRevLett.65.960).

- [53] A. Mirizzi, G. G. Raffelt, P. D. Serpico. Photon-axion conversion in intergalactic magnetic fields and cosmological consequences. *Lect. Notes Phys.* **741** (2008) pp. 115-134. ePrint [arXiv:astro-ph/0607415v1](https://arxiv.org/abs/astro-ph/0607415v1) .
- [54] R. Gill, J.S. Heyl. Constraining the photon-axion coupling constant with magnetic white dwarfs. *Phys. Rev. D* **84**, 085001 (2011); DOI: [10.1103/PhysRevD.84.085001](https://doi.org/10.1103/PhysRevD.84.085001)
- [55] Javier Redondo, Andreas Ringwald. Light shining through walls. DESY 10-175, MPP-2010-149 (2010); DOI: [10.1080/00107514.2011.563516](https://doi.org/10.1080/00107514.2011.563516)
- [56] K. van Bibber *et al.* Proposed experiment to produce and detect light pseudoscalars. *Phys. Rev. Lett.* **59** 759 (1987); DOI: [10.1103/PhysRevLett.59.759](https://doi.org/10.1103/PhysRevLett.59.759)
- [57] K. Ehret *et al.* New ALPS Results on Hidden-Sector Lightweights. *Phys. Lett.* **B689** pp. 149-155 (2010); ePrint arXiv:1004.1313v1.
- [58] J. Redondo. Can the PVLAS particle be compatible with the astrophysical bounds? (2008); ePrint [arXiv:0807.4329](https://arxiv.org/abs/0807.4329) s
- [59] L. Maiani *et al.* Effects of Nearly Massless, Spin Zero Particles on Light Propagation in a Magnetic Field. *Phys. Lett.* **B175** (1986) pp. 359-363; DOI: [10.1016/0370-2693\(86\)90869-5](https://doi.org/10.1016/0370-2693(86)90869-5)
- [60] Y. Semertzidis *et al.* Limits on the production of light scalar and pseudoscalar particles. *Phys. Rev. Lett.* **64** (1990) 2988; DOI: [10.1103/PhysRevLett.64.2988](https://doi.org/10.1103/PhysRevLett.64.2988)
- [61] PVLAS Collaboration, E. Zavattini et. al., Experimental observation of optical rotation generated in vacuum by a magnetic field, *Phys.Rev.Lett.* 96 (2006) 110406 [[hep-ex/0507107](https://arxiv.org/abs/hep-ex/0507107)].
- [62] PVLAS Collaboration (E. Zavattini *et al.* New PVLAS results and limits on magnetically induced optical rotation and ellipticity in vacuum. *Phys.Rev.* **D77** (2008) 032006; DOI: [10.1103/PhysRevD.77.032006](https://doi.org/10.1103/PhysRevD.77.032006)
- [63] P. Sikivie. Experimental tests of the invisible axion. *Phys. Rev. Lett.* **51** (1983) pp. 1415-1417; DOI: [10.1103/PhysRevLett.51.1415](https://doi.org/10.1103/PhysRevLett.51.1415).
- [64] T. Dafni. An update on the Axion Helioscopes front: current activities at CAST and the IAXO project. *Nuclear and Particle Physics Proceedings* **273–275** (2016) pp. 244–249; DOI: <http://dx.doi.org/10.1016/j.nuclphysbps.2015.09.033>.

- [65] D. M. Lazarus, *et al.*. Search for solar axions. *Phys. Rev. Lett.* **69** (1992) 2333; DOI: 10.1103/PhysRevLett.69.2333
- [66] R. Ohta, M. Minowa, Y. Inoue, Y. Akimoto, T. Mizumoto, A. Yamamoto. Prospects of Search for Solar Axions with Mass over 1 eV and Hidden Sector Photons. *RESCEU-50/09* (2009); ePrint arXiv:0911.0738v1.
- [67] Y. Inoue, Y. Akimoto, R. Ohta, T. Mizumoto, A. Yamamoto et. al., Search for solar axions with mass around 1 eV using coherent conversion of axions into photons, *Phys.Lett. B*668 (2008) pp. 93–97 [0806.2230].
- [68] CAST Collaboration (J. Ruz *et al.*) Recent Constraints on Axion-photon and Axion-electron Coupling with the CAST Experiment. *Phys. Procedia* **61** (2015) pp. 153-156; DOI: 10.1016/j.phpro.2014.12.025.
- [69] P. Sikivie, Experimental Tests of the Invisible Axion, *Phys.Rev.Lett.* **51** (1983) 1415.
- [70] R. Dicke. The Measurement of Thermal Radiation at Microwave Frequencies *Rev. Sci. Instrum.* **17** (1946) 268; DOI: 10.1063/1.1770483
- [71] T.M. Shokair *et al.* Future Directions in the Microwave Cavity Search for Dark Matter Axions. *Int. J. Mod. Phys. A***29** (2014) 1443004; DOI: 10.1142/S0217751X14430040.
- [72] E.W. Weisstein. Fast Fourier Transform. From MathWorld—A Wolfram Web Resource. Available online: <http://mathworld.wolfram.com/FastFourierTransform.html>. Accessed 3 Nov 2016.
- [73] van Bibber K, Kinion S. Experimental searches for galactic halo axions. *Phil. Trans. Roy. Soc. Lond. A***361**:2553 (2003); DOI: 10.1098/rsta.2003.1292
- [74] S. DePanfilis *et al.* Limits on the Abundance and Coupling of Cosmic Axions at  $4.5 < m_A < 5.0 \mu\text{eV}$ . *Phys. Rev. Lett.* **59** 839 (1987); DOI: 10.1103/PhysRevLett.59.839
- [75] C. Hagmann *et al.* A second generation cosmic axion experiment. *FERMILAB-CONF-95-416-A*, UCRL-JC-120869, C95-01-21. (1995); ePrint arXiv:astro-ph/9508013.
- [76] L.J. Rosenberg. Dark-matter QCD-axion searches. *Proc. Nat. Acad. Sci.* (2015); DOI: 10.1073/pnas.1308788112

- [77] S. J. Asztalos *et al.* SQUID-Based Microwave Cavity Search for Dark-Matter Axions. *Phys. Rev. Lett.* **104**, 041301 (2010); DOI: 10.1103/PhysRevLett.104.041301.
- [78] ADMX Collaboration (Asztalos, S.J. et al.) *Nucl. Instrum. Meth.* **A656** (2011) 39-44; DOI: 10.1016/j.nima.2011.07.019.
- [79] ADMX Collaboration (S. Asztalos *et al.* A SQUID-based microwave cavity search for dark-matter axions. *Phys. Rev. Lett.* **104** (2010) 041301; DOI: 10.1103/PhysRevLett.104.041301.
- [80] M. R. Buckley and H. Murayama, Quark mass uncertainties revive Kim-Shifman-Vainshtein-Zakharov axion dark matter. *JCAP* **0707** (2007) 012; DOI: 10.1088/1475-7516/2007/07/012.
- [81] Z. Ahmed *et al.* (CDMS Collaboration). Search for Axions with the CDMS Experiment. *Phys. Rev. Lett.* **103** (2009) 141802; DOI: 10.1103/PhysRevLett.103.141802.
- [82] E. Paschos, K. Zioutas. A Proposal for solar axion detection via Bragg scattering. *Phys. Lett. B* **323** (1994) pp. 367–372; DOI: 10.1016/0370-2693(94)91233-5
- [83] COSME Collaboration Collaboration (A. Morales *et al.*) Particle dark matter and solar axion searches with a small germanium detector at the Canfranc Underground Laboratory. *Astropart. Phys.* **16** (2002) pp. 325–332; DOI: 10.1016/S0927-6505(01)00117-7.
- [84] SOLAX Collaboration Collaboration (I. Avignone *et. al.*) Experimental search for solar axions via coherent Primakoff conversion in a germanium spectrometer. *Phys. Rev. Lett.* **81** (1998) pp. 5068–5071; DOI: 10.1103/PhysRevLett.81.5068.
- [85] R. Bernabei *et al.* Search for solar axions by Primakoff effect in NaI crystals. *Phys. Lett.* **B515** (2001) pp. 6–12. DOI: 10.1016/S0370-2693(01)00840-1.
- [86] The XENON100 Collaboration (E. Aprile et al.) First Axion Results XENON100 Experiment. *Phys. Rev. D.*, **90** (2014); ePrint arXiv:1404.1455v2.
- [87] XMASS collaboration (K. Hiraide). XMASS: Recent results and status. Conference: C15-02-11 (2015); e-Print: arXiv: 1506.08939.

- [88] The XMASS Collaboration (K. Abe *et al.*) Search for solar axions in XMASS, a large liquid-xenon detector. *Phys. Lett. B* **724** (2013) pp. 46-50; DOI: 10.1016/j.physletb.2013.05.060.
- [89] R. Bahre. Any light particle search II — Technical Design Report. DESY 13-030 (2013); DOI: 10.1088/1748-0221/8/09/T09001.
- [90] P. Arias *et al.* WISPy Cold Dark Matter. *JCAP* 1206 (2012) 013. (2012); DOI: 10.1088/1475-7516/2012/06/013.
- [91] E. Armengaud *et al.* Conceptual Design of the International Axion Observatory (IAXO). FERMILAB-PUB-14-476-A, BNL-106253-2014-JA; ePrint arXiv:1401.3233.
- [92] IAXO Collaboration (Irastorza, Igor G). The International Axion Observatory IAXO. Letter of Intent to the CERN SPS committee. CERN-SPSC-2013-022. SPSC-I-242 (2013) CERN-SPSC-2013-022; Available online: <http://cds.cern.ch/record/1567109>.
- [93] ADMX Collaboration. Available Online: <http://depts.washington.edu/admx/future.shtml>. Accessed 3rd Nov 2016.
- [94] D.J.E Marsh. Axion Cosmology. *Physics Reports* **643** (2016) pp. 1–79; DOI: 10.1016/j.physrep.2016.06.005.
- [95] J. Miller *et al.* Prospects for doubling the range of Advanced LIGO. *Phys. Rev. D* **91** (2015) 062005; DOI: <https://doi.org/10.1103/PhysRevD.91.062005>.
- [96] H. Grote *et al.* First Long-Term Application of Squeezed States of Light in a Gravitational-Wave Observatory. *Phys. Rev. Lett.* **110** (2013) 181101; DOI: 10.1103/PhysRevLett.110.181101.
- [97] B.M. Brubaker *et al.* First results from a microwave cavity axion search at 24 micro-eV. (2016); e-Print: arXiv: 1610.02580.
- [98] D. Budker *et al.* Cosmic Axion Spin Precession Experiment (CASPER). *Phys. Rev. X* **4** 021030 (2014); DOI: 10.1103/PhysRevX.4.021030
- [99] P.W. Graham and S. Rajendran. New observables for direct detection of axion dark matter. *Phys. Rev. D* **88** 035023 (2013); DOI: [doi.org/10.1103/PhysRevD.88.035023](https://doi.org/10.1103/PhysRevD.88.035023).

- [100] The DEAP Dark Matter Experiment *DEAP Dark Matter Experiment using Argon Pulse-shape discrimination*. [Online] Available from: <http://deap3600.ca/> [Accessed 10th June 2015].